Solvated Electrons on Metal Oxide Surfaces

Jin Zhao, Bin Li, Ken Onda, Min Feng, and Hrvoje Petek*

Department of Physics and Astronomy, University of Pittsburgh, Pittsburgh, Pennsylvania 15260

Received June 22, 2006

Contents

1. Introduction

An electron added to a solvent polarizes its surrounding medium to minimize the free energy. Such an electron with its polarization cloud, which we refer to as the solvated electron, is one of the most fundamental chemical reagents of significant experimental and theoretical interest. The structure and dynamics of solvated electrons in protic solvents have been explored ever since the discovery of intense blue coloration in solutions of alkali metals in ammonia.[1−3] Because solvated electrons are the most fundamental chemical reagents as well as carriers of negative charge, substantial experimental and theoretical efforts have focused on elucidating their equilibrium structure and solvation dynamics in a variety of neat liquids.[4,5] One of the most important but least explored environments for solvated electrons, namely, the two-dimensional liquid/solid and liquid/vacuum interfaces, is the subject of this review.

Solvated electrons can be introduced into protic solvents through the dissolution of highly reducing species such as alkali metals or through the exposure of liquids to ionizing radiation.[6,7] Transient chemistry of solvated electrons in water and other protic solvents has been studied extensively through radiochemical techniques.[3,4] More recently, it has became possible to inject excess electrons into solvents by means of ionization of precursor ions or molecules with femtosecond lasers or to excite solvated electrons into higher lying electronic states. Strong perturbation to the equilibrium solvent structure can be achieved by optically exciting solvated electrons from their s-symmetry ground state to the triply degenerate p-symmetry first excited states or even to the conduction band (CB) of the solvent (Figure 1). Because optical excitation is faster than the nuclear motion, the spherically symmetric distribution of the ionic cores in the ground state cannot adiabatically follow the change in the symmetry and spatial extent of the electronic wave function. Thus, optical excitation nonadiabatically projects the spherically symmetric solvent ionic core distribution onto the anisotropic distribution of the first excited state or the isotropic distribution of the CB (Figure 1). The projection of the ground-state wave packets onto these excited states turns on suddenly electrostatic forces on the molecular dipoles, which respond to screen the new charge distribution. The screening starts through inertial vibrational and translational motion of the inner shell solvent molecules. After the dissipation of the primary forces, a more gradual diffusive dielectric response of the solvent further stabilizes the excited state and eventually returns electrons back to their ground state on femtosecond to picosecond time scales.[5]

Although much knowledge has been gained concerning the properties of solvated electrons in homogeneous media through studies of their chemistry, spectroscopy, and ultrafast interactions with the host solvent, much less is known about their properties in inhomogeneous media such as liquid/solid and liquid/vacuum interfaces. Electron transfer through liquid/solid interfaces is fundamental for many scientifically interesting, economically significant, and environmentally

* To whom correspondence should be addressed. E-mail: petek@pitt.edu.

10.1021/cr050173c CCC: $59.00
Published on Web 09/13/2006

Jin Zhao received her B.S. degree in physics from the University of Science and Technology of China (USTC) in 1998. Subsequently, she completed her Ph.D. work with Prof. J. G. Hou and Prof. Jinlong Yang in 2003 at USTC. For the Ph.D. degree, she mainly worked on the theoretical research of the electronic properties of small molecules and nanoclusters in cooperation with STM experiments. In March 2004, she joined the research group of Prof. Hrvoje Petek at the University of Pittsburgh. The focus of her research in Pittsburgh is the theoretical study of the electronic structure and ultrafast dynamics of solvated electrons on metal oxide surfaces.

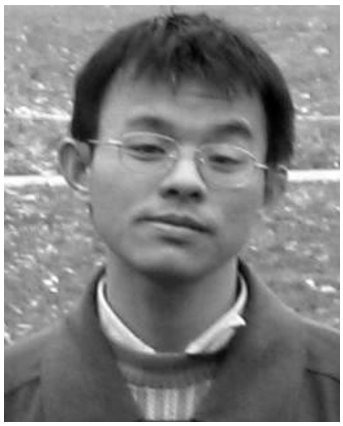

Bin Li was born in Sichuan, China (1976). He received his B.S. degree in applied physics from Department of Technique Physics at Peking University (Beijing, China) in 1999 and his M.S. degree in physics from Department of Physics and Astronomy at the University of Pittsburgh (PA) in 2000. He has been a doctoral student in Professor Hrvoje Petek's ultrafast dynamics research group at University of Pittsburgh since 2001, where he is mainly performing time-resolved photoemission experiments, and anticipates completing his Ph.D. (2006) in chemical/optical physics. His research interests include ultrafast laser technology, optoelectronic device control, surface spectroscopy and photochemical reactions, electronic structures, and charge-transfer dynamics on metal oxides or in heterogeneous systems.

pervasive phenomena such as electrochemistry, catalysis, photocatalysis, corrosion, sensing, prebiotic chemosynthesis, etc.[8−19] The structure of a liquid/solid interface is governed by specific solvent−surface and solvent−solvent interactions, as well as the electronic polarization of the interface region.[20−26] The interface presents a special 2D dielectric environment for the solvation of excess charge, where less solvent is available to polarize and the solvation energy is smaller than in the fully 3D environment of a solution.[11,24,27,28] Therefore, the liquid/solid interface can form a free-energy barrier for the transfer of electrons between the two media, where the properties of the interface and fluctuations of the solvent can influence the potentials required to drive chemical reactions.[14,17]

Ken Onda was born in Tokyo, Japan, in 1964. He received his B.A. degree in 1989 from the International Christian University and M.S. degree in 1991 from the University of Tokyo. He completed his Ph.D. thesis with Professor Kaoru Yamanouchi at the University of Tokyo in 1994. In 1995, he became a research associate of Professor Chiaki Hirose's laboratory at the Tokyo Institute of Technology. In 2002, he joined the research group of Professor Hrvoje Petek at the University of Pittsburgh. Since 2004, he has been a researcher of Koshihara Non-Equilibrium Dynamics Project, Japan Science and Technology Agency. His current research interests include the ultrafast chemical dynamics on oxide surfaces and the ultrafast photoinduced phase transitions in organic conductors.

By means of optical excitation, it is now possible to induce vertical interfacial charge-transfer excitation, where excess electrons are injected into the interfacial solvent overlayer faster than the ionic cores of the solvent can respond to the charge redistribution.[29−31] When the femtosecond laser excited nonlinear two-photon time-resolved photoemission (TR-2PP) is combined with surface science sample preparation techniques, it is possible to prepare atomically ordered solvent overlayers on single-crystalline surfaces and to study the ultrafast dielectric response initiated by the photoinduced interfacial charge transfer.[32−36] The evolution of the injected electron momentum, energy, and population on account of dynamical processes such as the coherent transport through the molecular overlayer, the localization through the charge-induced structural reorganization (polaron formation), the diffusive solvation, and the decay through the reverse transfer to the solid substrate can be investigated across more than 15 orders of magnitude in time.[37−43] A broad spectrum of interactions of excess electrons injected into dielectric media has been investigated for overlayer films of rare gas atoms,[44−49] aliphatic and aromatic hydrocarbons,[29,38,50−55] polar solvents,[56] and protic solvents[30,31,57−63] on metal and metal oxide substrates. TR-2PP provides unprecedented access to the primary inertial response of dielectric interfaces on femtosecond time scales that is difficult to attain in the conventional bulk or cluster studies of electron solvation.[31] Here, we review the recent TR-2PP studies of electron solvation in protic solvents (H_2O and CH_3OH) on metal and metal oxide surfaces, with the primary focus on charge-transfer dynamics relevant to the photocatalysis on TiO_2.[64−67] Extensive reviews of the structure and chemistry of water/solid and water/vacuum interfaces that are important to the present discussion have been a subject of recent special topic issues of *Chemical Reviews* and *Current Opinion in Solid State and Materials Science*.[19−26]

Because many aspects of the extensively studied 3D solvation of electrons are relevant to the solvation at interfaces, we begin this review in section 2 with a discussion of the molecular and electronic structure of solvated and CB electrons in H_2O. Of particular interest are recent studies on

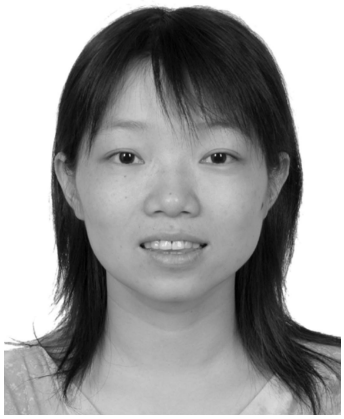

Min Feng received her B.S. and M.S. degrees from the South-West Petroleum Institute in the south of China and her Ph.D. degree from the Institute of Physics, Chinese Academy of Science. After completion of her Ph.D. in 2005, she joined the group of Professor Hrvoje Petek at the University of Pittsburgh as a postdoctoral researcher. Her research in the Laboratory of Ultrafast Dynamics centers on the electronic structure and dynamics at the molecule/solid interface.

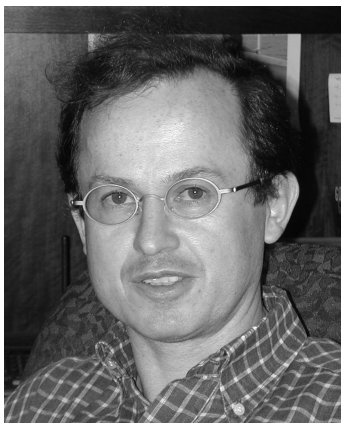

Hrvoje Petek was born in Zagreb, Yugoslavia, and raised in Amherst, New York, where he studied molecular spectroscopy with R. W. Field as an undergraduate student at MIT and with C. B. Moore as a graduate student at U. C. Berkeley. During his 15 year sojourn in Japan, first as a postdoctoral fellow and a Research Associate at the Institute for Molecular Science, he mastered the arts of ultrafast spectroscopy with K. Yoshihara, and later as a Group Leader at Hitachi Advanced Research Laboratory, he brought these skills to studies of ultrafast surface dynamics. In 2000, he became a Professor of Physics at the University of Pittsburgh, where he is now also the co-Director of the Petersen Institute for NanoScience and Engineering. He is the inventor of the interferometric time-resolved photoemission spectroscopy and photoemission electron microscopy, which have made possible studies of the electronic dephasing in metals, the nuclear motion of atoms and molecules in surface femtochemistry, and recording of attosecond movies of nanometer spatial scale electron dynamics. Petek was an Alexander von Humboldt Senior Scholar and is a Fellow of the American Physical Society. From July of 2006, he has been appointed Editor-in-Chief of Progress in Surface Science. The research reported herein represents the results of his first graduate student at the University of Pittsburgh, Dr. Bin Li.

size-selected water anion clusters, where the favorable surface/volume ratio makes the coexistence of surface and bulk solvation possible, although the interpretation of experimental data is still controversial.[68,69] In section 3, we compare and contrast the structure of H_2O overlayers on metal and metal oxide surfaces. Although this subject has been recently reviewed, we focus on structural aspects that are particularly relevant to the interfacial electron solvation and electron-transfer dynamics. In section 4, we present the recent studies of Bovensiepen and Wolf and co-workers on

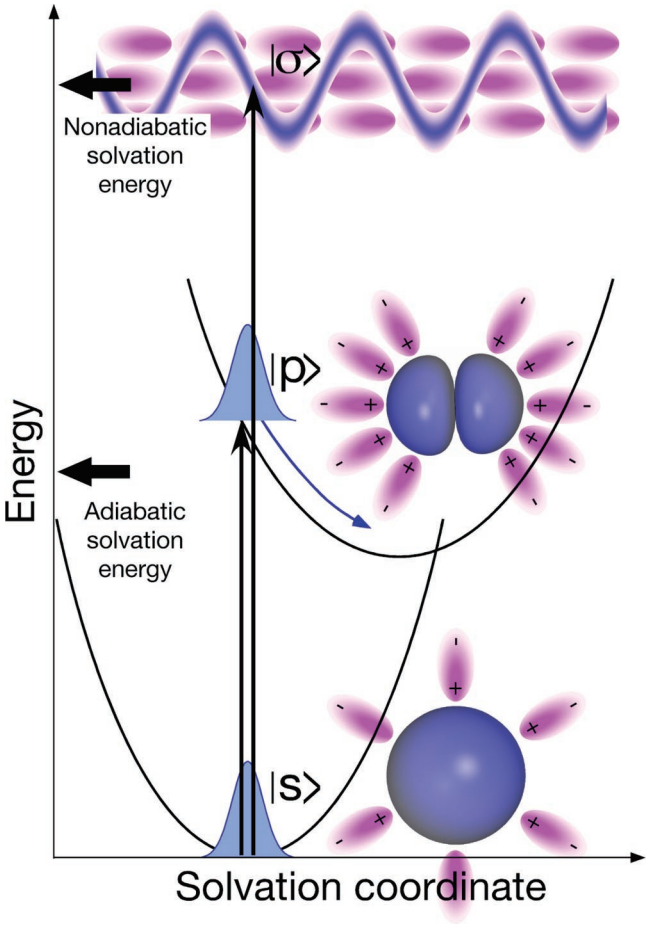

Figure 1. Energy diagram for the solvation and electronic excitation of excess electrons in water. Horizontal arrows mark the adiabatic (1.5−1.7 eV) and nonadiabatic (3.2 eV) solvation energies. The vertical arrows indicate p ← s absorption and photoemission experiments, which occur nonadiabatically with the ionic cores frozen during the excitation process. The nonadiabatic solvation energy corresponds to the photoemission threshold as well as the CB of H_2O. The optical p ← s excitation leads to a displacement along the inertial solvation coordinate involving H_2O libration.

the electron solvation in crystalline and amorphous ice on metal surfaces, where parallels can be drawn to the bulk and cluster solvation studies.[41] By contrast, the electron solvation in H_2O and CH_3OH overlayers on TiO_2 described in section 5 is purely an interfacial phenomenon that is derived from the presence of the minority surface −OH species.[31,62] Finally, in section 6, we conclude and provide an outlook for this rapidly evolving field.

2. Structure and Dynamics of Solvated Electrons

The introduction of excess electrons strongly perturbs the liquid structure within its screening volume. As shown in Figure 1, electrons in molecular solvents are known to exist in three characteristic states: they can be confined to a solvent cavity of approximately spherical symmetry that provides the maximum stabilization; they can be excited to p-symmetry excited states, which are unstable with respect to the s-symmetry ground state and have exceedingly short lifetimes; or they can exist transiently as delocalized waves in the CB of the solvent. Optical transitions between different electronic states occur nonadiabatically, requiring the solvent to assume different structures following the excitation to accommodate the change in the electron wave function. The

reorganization of the solvent occurs through the inertial and diffusive molecular motion on femtosecond to picosecond time scales.

2.1. Structure of Water

Protic solvents, such as H_2O, which form hydrogen-bonding networks, experience particularly pronounced perturbation of their equilibrium structure through the introduction of an excess charge.[70−78] In liquid water and ice, each H_2O molecule acts both as a proton donor and acceptor to form up to four hydrogen bonds (HBs). To form the HB network, two lone-pair electron orbitals on each O atom are pulled out by electropositive H atoms of two neighboring molecules, while the intramolecular bond lengths increase by 2% with respect to isolated molecules on account of the charge transfer that accompanies hydrogen bonding.[70] These electronic polarization and charge-transfer interactions increase the dipole moment of water from 1.86 D in the gas phase to ~3 D in liquid phase. According to the experimentally determined X-ray structure factor of water, upon forming the HB network, an electron charge of approximately 0.5*e* is transferred along each O−H bond of water molecules, leading to a substantially larger dipole moment than in the gas phase.[71]

The structure of water has been investigated by a variety of sophisticated experimental and theoretical techniques.[71,75,76,79] X-ray and neutron diffraction studies provide radial distribution functions for H and O atoms that define the average HB structure of liquid water and ice. According to a theoretical interpretation of these studies, the most probable intermolecular O−H bond length in liquid water is 0.96 Å, while the O···H HB is 1.8 Å. Furthermore, the O−O radial distribution function R_{O-O} peaks at 2.76 Å, while the HB angle distribution peaks at 180°.[73]

The addition of excess electrons to liquid water elicits major reorganization of the local liquid structure (solvation) to minimize the free energy of the system. The electropositive H atoms of water are attracted to the negative charge, while the electronegative O atoms are repelled. The strength of the interaction of H atoms with the excess electrons is comparable to the HB with the proximate O atoms in the pre-existing HB network of water. The electrostatic interaction of the excess electron with the H_2O dipoles leading to the formation of e^-···H−O "bonds" at the cost of disrupting the existing HB network provides the thermodynamic driving force to reorganize locally the structure of water.[80,81] The adiabatic energy of solvation, i.e., the energy released by solvating an electron at rest along the minimum free-energy pathway, which is difficult to obtain directly from an experiment, has been estimated from indirect measurements and theory to be from ~ −1.5 to −1.7 eV.[81,82] The energy diagram for the electronic excitation, adiabatic and vertical electron solvation, and photoemission in H_2O is given in Figure 1.[83]

Significant information on electron solvation in H_2O has been obtained through vertical excitation of electrons in liquid, cluster, and interfacial environments.[5,30,31,57−62,84−92] The creation of free electrons in water either through ionization of neat solvent or other more easily ionized parent species or through charge-transfer excitation from a solid substrate injects the excess charge faster than the solvent molecules can respond. The solvation process proceeds initially through the inertial motion of the solvent involving mainly the solvent libration on ~50 fs time scale,[5,93] which disrupts the existing HB network to create multiple H atom acceptor sites. The deuterium isotope effect on solvation, which scales with the square root of the reduced mass for libration, implicates the inertial reorientation H_2O molecules as the primary event in the electron solvation.[87,92,93] The prompt inertial response is followed by slower diffusional motion, which provides additional screening of the charge and also heals the disrupted HB network. For viscous solvents (glasses) such as H_2O ice, the energetic barriers to be overcome as the system approaches thermal equilibrium can stretch the diffusional component over more than 15 orders of magnitude in time.[43]

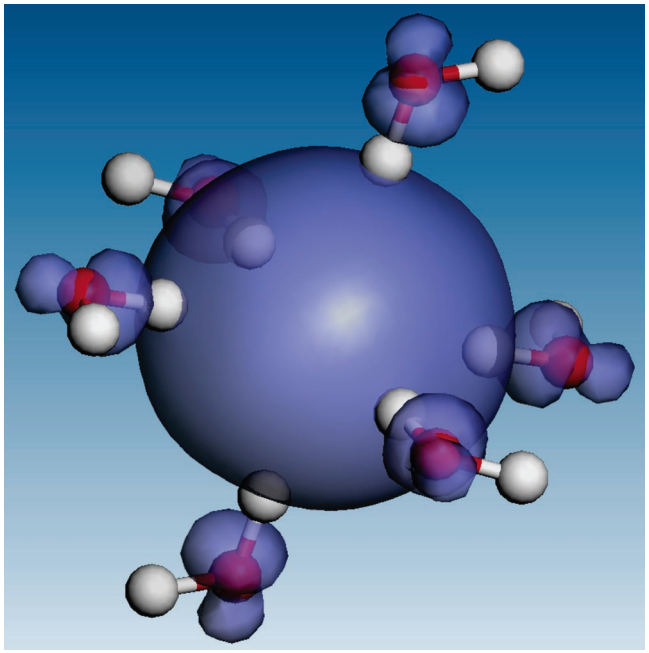

Figure 2. Kevan structure for the electron solvation in water calculated for six water molecules. O atoms are indicated in red, and H atoms are indicated in white. The blue translucent orb represents the solvated electron probability density.

2.2. Structure of the Hydrated Electron

2.2.1. Kevan Structure of the Solvated Electron

The equilibrium structure of solvated electrons in water (hydrated electrons) has been studied extensively by both experiment and theory. The Kevan structure, which is most widely accepted, has been proposed to explain the ESR spectra of solvated electrons in H_2O.[94] Theoretical calculations that treat the electron as a quantum mechanical particle and water molecules as rigid classical particles using empirical models for the water−water and water−electron interactions reproduce the Kevan structure and the associated solvated electron spectrum.[94−99] In the Kevan structure, such as shown in Figure 2, electrons are trapped within a dynamically fluctuating but on the average spherically symmetric molecular cavity with a radius of ~2.4 Å formed by a primary solvation shell of approximately six octahedrally distributed H_2O molecules contained within a sphere of a 4 Å radius. Radial distribution functions from quantum simulations of the hydrated electron place the nearest H and O atoms 2.3 and 3.3 Å from the electron center of mass, respectively.[95] The proximate water molecules preferentially orient to point single O−H bonds into the electron center of mass rather than along the molecular dipole. The proximity

of H atoms to the electron cloud confirms their primary role in stabilizing the excess charge. In water and other protic solvents, these "dangling" H atoms, which do not partake in a strong HB with other electronegative species such as O atoms, are the most electropositive acceptor sites that stabilize the excess electron charge.[100] The interaction of these dangling H atoms with the excess electron charge is the main theme of this review.

The structures of solvated electrons in other protic solvents resemble the Kevan structure in H_2O. However, some differences can be attributed to the HB structure of the solvent, the alignment of the dipole moment, the size of the solvent, etc. The weaker strength of HBs and larger number of dangling H atoms make solvated electrons in ammonia significantly more stable than in water.[101] The presence of three acceptor sites for every donor site in ammonia molecules ensures that dangling H atoms are available to stabilize excess electrons even without breaking the existing HBs. The first solvation shell of ammonia consists of 6−9 molecules.[98,99,102,103] In alcohols, each OH species embodies two electron-donor and one electron-acceptor sites per molecule. Liquid methanol is composed of linear polymers of hydrogen-bonded chains.[104] The electron spin resonance (ESR) spectra of solvated electrons in CH_3OH are consistent with four molecules in the first solvation shell; however, molecular dynamics calculations predict a shell of six to seven molecules. The molecules align along the direction of the dipole moment, but because the dipole moment is to a large extent determined by the OH species, the alignment is also close to the direction of the O−H bond.[94,105] In addition to OH, the aliphatic H atoms on the methyl group (H_m) can form weak HBs and are also thought to participate in the stabilization of solvated electrons.[106,107]

However, the Kevan structure is not the only proposed structure of solvated electrons. Alternative structures for solvated electrons in H_2O and NH_3 based on ab initio and density functional theory (DFT) calculations have been proposed. Zhan et al. have concluded that a pair of strong and opposing $e^-\cdots$H−O bonds is responsible for the primary electron stabilization in the Kevan structure. In their structure, the first solvation shell still consists of six molecules, but approximately only two H_2O molecules contribute single H atoms to the peak at 2.3 Å in the radial distribution function of H atoms. Alternatively, the absorption and Raman spectra of the solvated electron in H_2O have been reproduced by structures involving the $OH^-\cdots H_3O$ complex.[108−112] Similar alternative structures have also been proposed for NH_3.[99]

2.2.2. Electronic Structure of Solvated Electrons

The intense blue color of solvated electrons in H_2O has been attributed to excitation from the s-symmetry ground-state Kevan structure to the triply degenerate p-symmetry excited state.[3] The absorption spectrum corresponding to the p ← s transition is centered at 720 nm (1.725 eV) and has an exceptionally broad bandwidth of 0.84 eV.[96,97,113−115] The line shape has a characteristic asymmetry that is often simulated by a Lorentzian profile on the high-frequency side and a Gaussian profile on the low-frequency side without a theoretical justification. However, Pshenichnikov et al. have successfully fit the asymmetric spectrum to a generalized Lorentzian function with a T_2 dephasing time of 1.6 fs that they obtained from time domain measurements.[5] They attributed the asymmetric line shape to the breakdown of the slowly varying envelope approximation for extremely fast dephasing times. However, similar line shapes are observed for a variety of spectroscopic measurements on solvated electrons in H_2O and other solvents even when narrower line widths justify the slowly varying envelope approximation,[83,115] which suggests that the asymmetry may have additional origins. For instance, Linder et al. interpreted the p ← s absorption spectrum of NH_3 within the framework of Kubo's stochastic theory of line shapes to capture the effect of structural fluctuations within the solvent shell on the modulation of the s−p gap.[98]

The vertical excitation of the p ← s transition changes the solvated electron wave function faster than the molecules forming the solvation shell can relax to new equilibrium positions. Upon excitation, the solvent molecules interacting with the excited excess electron experience a step-function force, which drives the solvent reorganization on the femtosecond to picosecond time scales.[5,85,86,88−92,116,117] In numerous experimental and theoretical studies, the observed spectrum and ultrafast solvation dynamics have been interpreted in terms of the distortion and subsequent recovery of the Kevan structure. However, transient absorption and nonlinear diffraction measurements have been interpreted by two different models for the internal conversion to the ground state. Barbara and co-workers attributed the initial, deuterium-isotope-dependent changes in the transmission spectra following the p ← s excitation to the adiabatic solvation through the inertial libration of the solvent on the 35−80 fs time scale, which is followed by the nonadiabatic internal conversion to the ground state on the 200−300 fs time scale.[86,87] Pshenichnikov et al. do not find evidence in the primary relaxation dynamics for the stabilization of the excited state through adiabatic solvation. Instead, they attribute their 50 (70) fs transients to the coupling of the p state in H_2O (D_2O) to a conical intersection with the s state via the inertial libration of solvent molecules in the first solvation shell.[5,92]

The excited p-state solvation dynamics have also been studied for NH_3, CH_3OH, and longer alcohols.[98,99,118,119] The internal conversion from the p state in NH_3 is reported to be too fast to observe with ∼100 fs time resolution.[98] By contrast, the p state in methanol with a lifetime of ∼300 fs is considerably more stable.[119] The higher stability of the p state of solvated electrons in methanol may be related to the different nature of the inertial solvent response[105,120,121] and possibly to the larger s−p band gap of 1.94 eV.[122]

Theoretical simulations concur that the librational motion is the primary mode of the inertial component of solvation in water. However, in other solvents such as methanol, both the density and frequency of librational modes are lower and, therefore, translational motion is thought to dominate the inertial solvation.[105,120,121,123−125] Consequently, the solvation dynamics in methanol are substantially slower than in water.[122,126,127]

2.2.3. CB of Water

Although the near-infrared p ← s absorption spectra of solvated electrons in water and other solvents have been the primary focus in the discovery of solvated electrons and the studies of their solvation dynamics, related spectral features have been predicted[128] but not yet observed on water-covered solid surfaces. Instead, in the studies of 2D solvation in adsorbate films on solid surfaces, the CBs of water and other solvents have been exploited as the primary conduits for the injection of electrons into the molecular overlayer.[29,30] Electrons are efficiently introduced into the CB of H_2O

overlayers through injection from either the substrate or the vacuum side. This can be accomplished either by charge-transfer photoexcitation with >3.0 eV photons[29,30] or by irradiation of the sample with near-zero kinetic energy electrons from vacuum.[129] Tunneling electrons from appropriately biased scanning tunneling microscopy (STM) tips can also be injected into CBs of molecular overlayers.[130,131]

Unlike the solvated electrons, the CB electrons are delocalized within the bulk or interfacial molecular networks.[90,132,133] CB electrons are unstable with respect to the solvated electrons because local static or dynamic fluctuations of the solvent can create an attractive potential and progressively localize them to form a more stable polaron, of which an extreme case is the Kevan structure.

The vertical excitation energy from the Kevan structure to the CB of water is difficult to establish experimentally. The $(H_2O)_n^-$ cluster studies give 3.25 eV as the asymptotic energy for the vertical ionization in the limit of large clusters.[69,83] The photoemission threshold energy and the CB energy are considered to be the same under the assumption that bulk H_2O has negative or negligibly small electron affinity in a sudden process, such as photoemission, where the molecular lattice is frozen.[4,69,83,90] However, the uncertainty in the vertical ionization energy is large and subject to the interpretation of broad Lorentzian−Gaussian photodetachment line shapes.[83] In liquid water, 400 nm of light (3.16 eV) is sufficiently energetic to detrap electrons from the Kevan structure.[132]

In the reverse process of trapping, the excess energy of CB electrons is dissipated through the formation of the Kevan solvation structure at the cost of disrupting locally the existing HB network and localizing electrons within the solvent cavity.[95] The trapping and relaxation of CB electrons to the vibrationally hot ground state in liquid H_2O is reported to occur on the 300-400 fs time scale.[90,133] The solvation of the CB electrons apparently proceeds without appreciable population of the shorter lived intermediate p-symmetry excited state.[5,92] The slower solvation time for the CB electrons in comparison with the p state has been attributed to their more significant delocalization.[133]

2.3. Water Cluster Anions

Molecular cluster anions provide another versatile environment where electron solvation can be studied through cluster-size selection over a range from the single molecule to the near-bulk solvent limits.[69,83,134−137] The large surface/bulk ratio makes it possible, in principle, to study both surface and bulk solvation for the same range of cluster sizes and experimental conditions. The smallest $(H_2O)_n^-$ cluster to bind an electron through dipolar forces is the water dimer.[138,139] The smallest $(H_2O)_n^-$ clusters possess only surface solvation sites, but as the cluster size increases, the number of possible isomers as well as the number of possible binding sites rapidly increase. The experimental characterization of small ($n \leq 6$) clusters, which are theoretically tractable,[100,139−143] has proven to be experimentally challenging.[144] For the smallest clusters, both experiment and theory identify the dangling H atoms on cluster surfaces as the electron-acceptor sites.[100,139,144] The most stable clusters identified by both experiment and theory have two dangling acceptor sites on a single H_2O molecule, such as shown for the calculated electron distribution of an H_2O pentamer in Figure 3.[145]

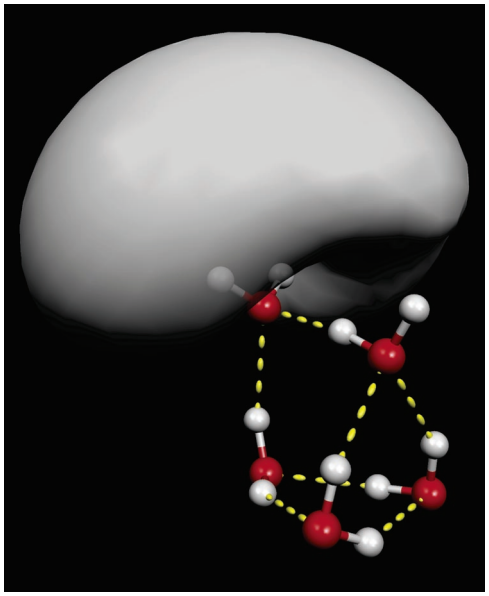

Figure 3. Excess electron distribution for a H_2O pentamer anion cluster from ref 145. A double acceptor molecule with two dangling H atoms pointing into the electron cloud presents the most stable binding site for the excess electrons. O atoms are indicated in red, and H atoms are indicated in white. Reprinted with permission from Science (http://www.aaas.org), ref 145. Copyright 2004 American Association for the Advancement of Science.

For larger clusters, both the surface and bulk solvation has been predicted by theoretical simulation and reported in experiments.[135,146] Path-integral molecular dynamics simulations predict that the surface-bound electrons are more stable for $n < 32$, and internally solvated electrons are favored for $n > 64$.[146] On the basis of the differences in the vertical electron-binding energy, Verlet et al. have identified two classes of clusters in the $n = 12-25$ regime, which they attribute to the surface- and bulk-bound isomers.[69] As the cluster size increases, the putative internal isomer vertical binding energy converges with the $n^{-1/3}$ dependence to the 3.25 eV photoelectric threshold of water.[83] For $n \sim 200$, the binding energy is still ~80% of its bulk value.[69]

However, the assignment of the isomer with the largest vertical binding energy to internally solvated electrons has been disputed on a theoretical basis; according to the simulations of Turi et al., the $n^{-1/3}$ scaling appears in the calculated binding energies only of the surface-solvated electrons.[68,147,148] Theoretical simulations predict similar stabilities for the surface- and bulk-solvated electrons.[27,68,149] However, the formation of excess dangling surface H atoms creates an electrostatic barrier for the penetration of electron into the bulk.[150] Consistent with this prediction, the formation of the putative internally solvated cluster anions is favored by conditions that favor relatively high cluster temperatures.[69]

The p ← s transition can also be excited internally or on surfaces of water clusters. Turi et al. predict that the transition energy for surface-bound electrons converges with the $n^{-1/3}$ dependence to the bulk value;[68] however, Rodriguez et al. predict a 0.52 eV red shift for electrons localized on the water/vacuum interface.[128] Bragg et al. found that the p-state relaxation rate increases with n^{-1} dependence to the bulk value of 50 fs for the interior-solvated clusters, while the rate is weakly size-dependent for the surface-solvated clusters.[69,151]

Cluster anion studies are important for the surface studies because they provide an important intermediate regime

between the 3D electron solvation in liquids and 2D solvation on solvent/solid or solvent/vacuum interfaces. The structural motifs that efficiently bind electrons to surfaces of small water clusters also are known to exist at H_2O/vacuum interfaces of both thin and thick (bulk) molecular films on solid surfaces.[21,23,152−156] In particular, structures that present one or two dangling H atom acceptor sites occur on solid surfaces either as a feature of perfect termination or as common surface defect sites. Furthermore, the issue of surface (e.g., the H_2O/vacuum interface) versus bulk solvation is also expected to have significant consequences on the structure and interfacial charge-transfer decay dynamics for electrons injected into thin molecular films on solids.[149,150] Surface-solvated electrons can be effectively decoupled from the CB of the substrate by the intervening H_2O layer if there is a barrier to surface−bulk conversion.

3. Water on Solid Surfaces

The presence of interfacial water on metal and metal oxide surfaces is of great consequence for many practical applications such as catalysis, corrosion, and other environmentally relevant processes.[12,20,157−160] In a broader context, interfacial water is vital in biological systems, where, for instance, it mediates charge transport and controls the structure and function of proteins.[20,161−163] The ability of water to transport charge can be controlled through its interactions with the protein or membrane interfaces.[164] Water donates charge to substrate atoms through its basic O atoms, and it accepts charge from the substrate through its acidic H atoms. The substrates are classified as either hydrophobic or hydrophilic depending upon how well they can accommodate these amphoteric interactions in the first adsorption monolayer and balance them with HB interactions in the subsequent monolayers.[25,26,165] Even if water wets the solid surface in the first monolayer, because of strong interactions with the substrate, the first overlayer may not offer a favorable growth template for the subsequent overlayers.

The hypothesis that the atomic structure and electrostatic fields of solid surfaces can be very favorable for adsorbing (condensing) water led to one of the earliest practical applications of surface science, namely, the seeding of rain clouds with crystal particles.[166,167] Even though many surfaces present favorable templates for the growth of water ice, determining the interfacial structure still is a challenge for both experiment and theory.[26,168−173] The structures are often determined by subtle effects that include the interaction potentials of O and H atoms with the substrate atoms, the intermolecular hydrogen bonding, and the competition between the associative versus dissociative chemisorption. Because these interactions are often of comparable magnitude and energy barriers may separate different chemisorption structures, subtle differences in the sample preparation or theoretical calculation can lead to different conclusions about the chemisorption structures of H_2O overlayers.[26]

3.1. Water Chemisorption on Metal Surfaces

Water interacts with metal surfaces primarily through its O atoms. The chemisorption of H_2O on metals typically decreases the work function on the order of 1.0−1.5 eV.[158] This change in the vacuum potential arises from the charge donation from the p orbitals of O atoms adsorbed at on-top sites to the d bands of metal substrates.[174] The interaction with H atoms is much weaker, although there is evidence for the back-donation from the substrate.[16] In comparison with the typical HB strength of water (∼0.25 eV), the interaction strength between H_2O is weaker for noble metals and comparable or stronger for transition metals.[26,175] Some surfaces such as Ru form strong bonds with the atomic H, which can lead to the partial dissociation of H_2O.[168,175,176] If the epitaxial relationship and the balance water−metal and HB interactions are favorable, water will self-assemble into crystalline HB networks.[26,177] On hexagonal symmetry surfaces, H_2O typically forms bilayer structures according to Bernal−Fowler−Pauling rules, such as in Figure 4, where a hexagonal H_2O lattice is formed by three H_2O molecules in the bottom layer binding to the surface with their O atoms, while the top three molecules interact primarily with the bottom layer molecules through HBs.[174] Such bilayer structures favor the epitaxial growth of the hexagonal I_h ice.[157,158,177] The shallow potentials for the translation and rotation of H_2O molecules with respect to the surface can accommodate epitaxial growth for a wide range of surface lattice parameters.[26] However, the fine balance between the aforementioned interactions, different surface preparation and analysis protocols, and ambiguous structural characterization techniques has led to a controversy concerning whether the molecular or dissociative H_2O chemisorption on Ru(001) is favored.[26,168−170,173−176,178,179] Careful experiments, which avoid electron-stimulated dissociation, have clearly established that D_2O chemisorbs molecularly when exposed to cold (<160 K) Ru(001) surfaces, while H_2O may partially dissociate into surface H and OH species.[60,171,176]

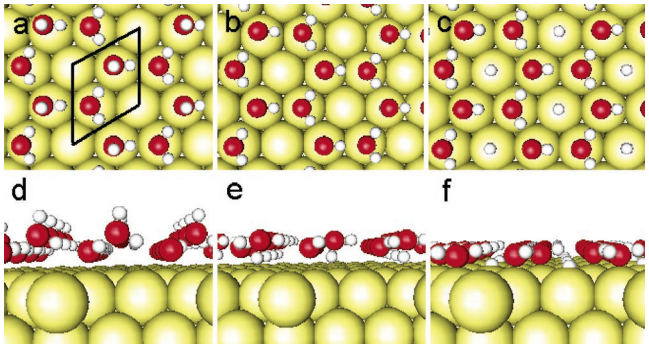

Figure 4. Calculated structure of (a and d) D up, (b and e) D down, and (c and f) half-dissociated structure of D_2O on the Ru(001) surface from ref 178. The $(\sqrt{3} \times \sqrt{3})R30°$ unit cell is marked in a. O atoms are indicated in red, and H atoms are indicated in white. Reprinted with permission from ref 178. Copyright 2005 Elsevier.

The interaction of water molecules with metal surfaces influences the structure of water overlayers and ultimately the process of electron solvation and interfacial charge transfer.[41] Within the bilayer structures, the molecular plane of the bottom layer molecules is typically near parallel to the metal surface. To form a bilayer structure, however, H atoms tilt up slightly to form the HBs with the top layer molecules. When the bilayer structure is formed, three H atoms of the top layer are locked into HBs, while three nonbonded H atoms remain. These have the choice of either pointing up into vacuum or down toward the surface, as shown in Figure 4. Because their energies are similar, both structures can coexist on a surface.[155,178] However, whether the dangling H atoms point up or down can strongly affect how H_2O overlayers accommodate excess electrons.[149,150]

The first bilayer forms the template for the growth of subsequent layers. Water on metals such as Ru(001) typically continues to form bilayer structures eventually forming I_h

crystalline ice.[58] Whether H_2O forms amorphous or crystalline films can be controlled by the growth and annealing conditions.[180] However, H_2O does not wet weakly interacting metals with a poor epitaxial relationship such as noble metals. Instead, H_2O forms 3D clusters at low coverages, which, at high coverage, condense into amorphous ice. Such amorphous ice can have a variable degree of porosity that depends upon the overlayer preparation conditions.[181] The resulting molecular-scale vacancies can act as electron-trapping sites.[58] The mode of growth of H_2O on metals can be controlled and established by standard surface science techniques such as temperature-programmed desorption (TPD), vibrational spectroscopy, STM, and electron or He atom diffraction.[21,26,60,152,177,180,182]

3.2. Water Chemisorption on Metal Oxides

The typical binding energy of H_2O molecules on metal oxide surfaces of ~1 eV greatly exceeds that on metal surfaces. The ionic metal oxide surfaces present much more corrugated electrostatic potential landscapes for the chemisorption of water than metals.[183,184] The arrays of Lewis acid (metal ion) and base (O ion) sites on metal oxides present highly singular templates for the chemisorption of H_2O.[159,183,185,186] Because these amphoteric interactions are typically stronger than the HB interaction among H_2O molecules, water can form structures in the first few monolayers that are substantially different from the common polymorphs of water ice.[187] As vivid contrasting examples of how the surface crystal templates of metal oxides self-organize different H_2O overlayers, Figure 5 presents the calculated structures of 1 monolayer (ML) H_2O-covered most stable rutile (110) and anatase (101) polymorph surfaces of TiO_2.[186,188]

As on metal surfaces, O atoms of water donate charge to the acidic metal ions of metal oxide substrates.[186,188] However, in contrast to metals, H atoms have the possibility of forming strong HBs with the basic O ions of the substrate in competition with the O atoms of neighboring water molecules.[186] The extent that H_2O molecules form intermolecular or molecule-surface bonds and their relative strengths very much depend upon the distribution of the acidic and basic surface sites and the strength of the interaction at each site. Dependent upon the geometry and dimensions of the lattice, molecule-surface or intermolecular HBs may be stronger. Only one, the other, or both types of HBs can form. Moreover, strong interaction with polar surfaces can lead to the dissociation of H_2O molecules.[182,189]

The surfaces of rutile and anatase polymorphs of TiO_2 highlight how the surface structure can lead to distinct H_2O overlayers. The rutile (110) surface in Figure 5a has a distance between five-coordinate terminal Ti^{4+}_{5c} ions of 2.96 Å, which is slightly longer than the 2.76 Å maximum in the R_{O-O} radial distribution function of H_2O. This slight mismatch favors the formation of both the molecule-surface and intermolecular HBs, with the former being stronger than the latter as judged by their relative bond lengths.[186] However, the $Ti^{4+}_{5c}-Ti^{4+}_{5c}$ distance of 3.79 Å found on the anatase (101) surface provides a registry that is of comparable dimension to the minimum in the R_{O-O} function of H_2O at 3.5 Å. As a consequence of the mismatch between the lattice dimension of anatase and the nearest neighbor distance in liquid water, only weak H_2O molecule-surface HBs can form.[187,188] Dependent on the degree to which the structure of a metal oxide surface can accommodate the molecule,

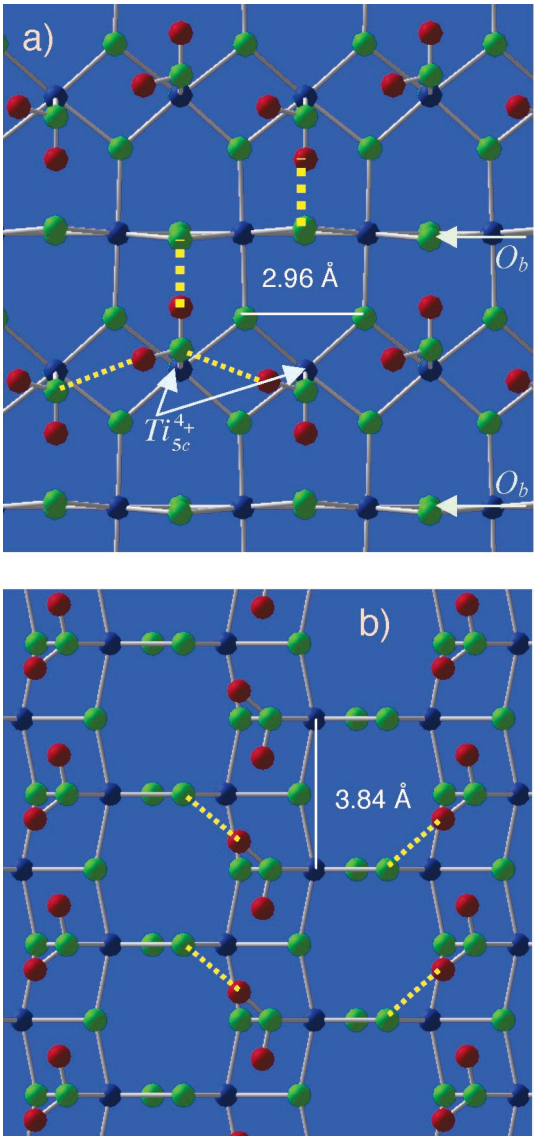

Figure 5. DFT-calculated structure of (a) rutile (110) and (b) anatase (101) H_2O/TiO_2 surfaces at 1 ML H_2O coverage. Arrows indicate specific sites discussed in the text. White lines indicate the relevant unit-cell dimensions. Dotted lines indicate strong (thick) and weak (thin) hydrogen bonds. Ti atoms are blue; O atoms are green; and H atoms are red.

surface and intermolecular HBs can have a strong impact on the strength of binding of the first and second H_2O overlayers.[158,190] On favorable surfaces, such as rutile (110), the additional molecule-surface HB interaction leads to stronger H_2O chemisorption than on metal surfaces.[191]

The surface-specific binding of H_2O molecules on metal oxides can be discerned from TPD measurements for rutile (110) and anatase (101) surfaces of TiO_2. For the rutile (110) surface, the first and second monolayers of H_2O desorb at 270 and 174 K, respectively, while for the anatase (101) surface, the corresponding processes occur at 250 and 190 K.[191−193] On rutile, the first monolayer interacts strongly with the available Ti and O sites of the substrate, which does not leave favorable sites (e.g., the dangling H atoms) for the interaction with the second monolayer. By contrast, the surface structure of anatase does not permit H_2O molecules bound through their O atoms to the Ti sites to form HBs with the neighboring first monolayer H_2O molecules. Because one H atom of each first monolayer molecule remains dangling, the second monolayer H_2O molecules can form

favorable HBs with the free H atoms of the first monolayer as well as with the O atoms of the substrate. The less favorable accommodation of the first monolayer H_2O and better accommodation of the second monolayer explains the difference in TPD results between the rutile (110) and anatase (101) surfaces.[188]

Although water dissociation is possible on metal surfaces, it is much more likely to occur on metal oxides.[182,189,194] Dissociative chemisorption readily occurs at O atom vacancy defects, which are usually the most common surface defect sites on metal oxides.[195] At defect sites, upon adsorption through its O atom, H_2O transfers a proton to a neighboring surface O atom to form two equivalent −OH species.[192,196−198] Such H atoms are usually highly mobile, especially in the presence of other H_2O molecules, allowing the dissociation products to disperse across the surface.[198]

The dissociative chemisorption can also occur on perfect metal oxide surfaces. In particular, when the surface metal and O atoms sites are strongly acidic and basic, respectively, H_2O molecules bound at the terminal metal sites can transfer protons to the proximate surface O atoms.[182,189,199] This forms two inequivalent OH species at the terminal metal and O atoms of the perfect surface.[189] Such dissociation of H_2O can drastically change the surface charge distribution and, therefore, is a common mode for the stabilization of polar oxide surfaces.[200]

Even if the dissociation of water on perfect metal oxide surfaces were exothermic, it could be suppressed by a large activation barrier.[189,201] Moreover, the dissociation of H_2O on metal oxides is often thermodynamically driven. Even though the dissociation may not be favorable under ultra high vacuum (UHV) conditions, as the vapor pressure of H_2O is increased, the equilibrium can be driven to the dissociated form.[202−204] Thus, under atmospheric conditions, metal oxides, which terminate most metal and mineral surfaces, are covered with an overlayer consisting of −OH and H_2O species.[183,203] The propensity of water to hydroxylate and wet metal oxide surfaces may make the formation of solvated electrons through optical or electron stimulation particularly significant in many environmental, geochemical, and practical applications.[183]

4. Electron Solvation in Molecular Overlayers on Metal Surfaces

Ordered or disordered molecular overlayers on solid surfaces present some of the most fascinating environments of great fundamental and practical significance for studying electron solvation dynamics.[41,42] By means of UHV surface science techniques, it is possible to form ordered molecular overlayers with single molecular layer precision on atomically ordered templates presented by solid surfaces. The molecular overlayer structure can be characterized on the atomic scale by a variety of structural probes, such as X-ray, electron, or He atom diffraction, real-space methods such as STM, or optical methods such as sum-frequency generation.[26] Such a highly ordered environment is ideally suited for studying the fundamental aspects of molecular solvation of electrons in two or three dimensions.

One of the great advantages of having atomically ordered molecular overlayers is the possibility of exploiting the full capabilities of experimental electronic structure methods such as photoemission to compare directly with calculations for periodic systems. In atomically ordered solids, atomic or molecular orbitals on adjacent lattice sites can hybridize to form delocalized bands. Such bands are described by energy−momentum dispersion functions, which define the effective electron mass for the propagation of electron waves through a solid and whose bandwidth is determined by the strength of interactions among the adjacent sites. Photoemission spectroscopy provides a powerful tool for mapping the band structures of solids, solid surfaces, and adsorbate overlayers on solid surfaces.[205,206]

The methods of photoemission spectroscopy can also be extended to the unoccupied states of solids. By means of ultrafast laser spectroscopy, it is possible to create a transient electron population in the unoccupied bands of the substrate or the molecular overlayer below and even above the vacuum level of the surface.[32,33,207] This population decays typically on the femtosecond time scale by either electro-electron ($e-e$) scattering or reverse charge transfer (RCT) from the overlayer into the resonant bands of the substrate. Before it decays, it is possible to probe the energy and population of the transient intermediate state with a time-delayed probe pulse, which further induces a transition from the intermediate states into the free-electron continuum above the vacuum level of the surface. The photoemitted electrons can be detected with energy and momentum resolution for single-pulse excitation or as a function of pump−probe pulse delay. By recording two-photon photoemission (2PP) spectra, it is possible to map out the dispersion functions of the unoccupied bands of the molecular overlayer or the substrate. Furthermore, time-resolved measurements on the unoccupied states reveal important dynamical details on the charge transport, localization, and the electron population and energy relaxation dynamics in the intermediate states.[41,42]

Because the fundamental aspects of TR-2PP spectroscopy have been presented in several excellent reviews,[32−34] we focus here mainly on those aspects that are relevant to the electron solvation in molecular overlayers. The mechanisms of molecular excitation on solid surfaces are still poorly understood. However, it is clear from most TR-2PP measurements that the main excitation process involves the direct substrate−adsorbate photoinduced charge transfer.[208,209] The initial states for the photoinduced charge transfer into the molecular overlayer can either be the bulk bands of the substrate or the surface states of the molecule-covered surface. The excitation can occur to a variety of unoccupied states of the adsorbate overlayer as long as they are connected by a transition dipole moment with the initial states of the substrate.

One of the main avenues for injecting charge into the adsorbate overlayer is through the image potential (IP) states of the interface.[39,210,211] On clean metal surfaces, the Coulomb interaction between electrons and their positive image charge forms an attractive IP, which converges to the vacuum level. Surface electrons are bound by the IP on the vacuum side and the crystal potential on the substrate side, to form a 2D Rydberg series that starts ~0.8 eV below the vacuum level for the principal quantum number $n = 1$ state (Figure 6a) and converges to the vacuum level for high n states. Because the electron density is mostly located in the vacuum, IP states disperse with parallel momentum from their minimum energy E_0 at $k_{||} = 0$ according to the $E = E_0 + (\hbar/k_{||})^2/(2m_{\text{eff}})$ dispersion relation with approximately the effective mass m_{eff} of a free-electron m_e. The electronic structure and relaxation dynamics of IP states on clean metal surfaces have been extensively studied by both experiment and theory, and they constitute one of the best understood aspects of the surface

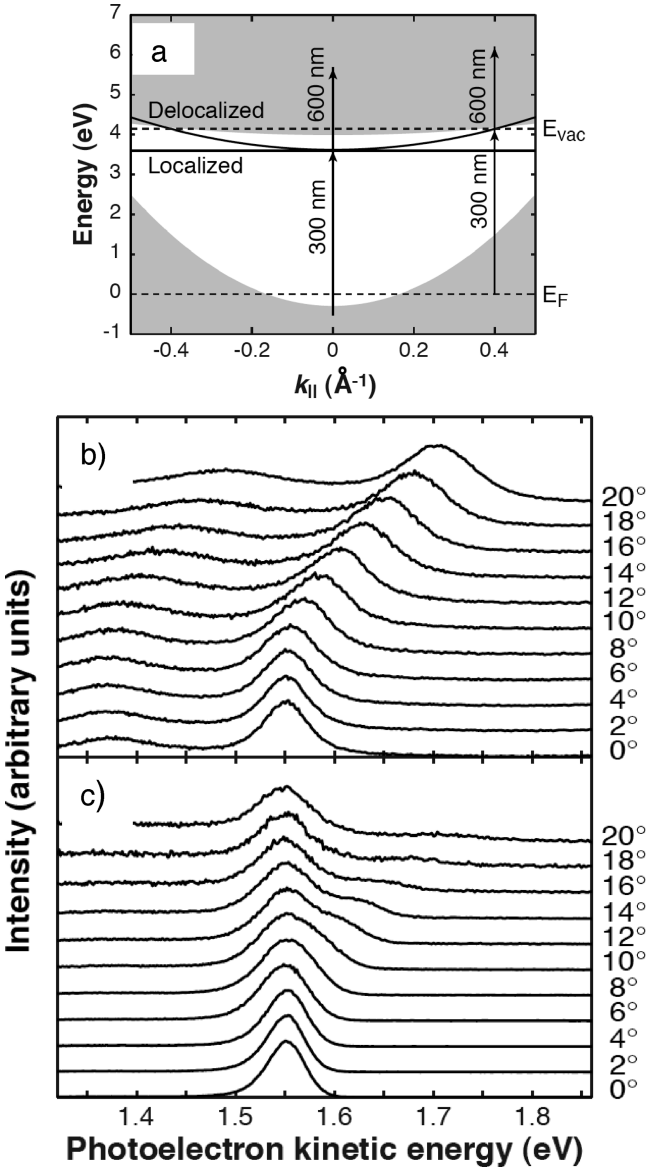

Figure 6. (a) Surface band structure dispersion with parallel momentum for *n*-heptane-covered Ag(111) surface and the 2PP excitation scheme. Delocalized $n = 1$ IP state disperses with $k_{||}$; however, the localized state following polaron formation does not. The unshaded area indicates ⟨111⟩ projected band gap of silver. Angle-resolved 2PP spectra from ref 29 for bilayer *n*-heptane−Ag(111) taken at 120 K sample temperature and a pump−probe delay time of 0 fs (b) and 1670 fs (c). Initially, the electron is in a delocalized state with an effective mass of $1.2m_e$. The electron then becomes localized within a few hundred femtoseconds through the polaron formation involving the distortion of the heptane overlayer. The smaller dispersive feature in b is from minority patches of the monolayer-covered surface interspersed with the bilayer. Reprinted with permission from Science (http://www.aaas.org), ref 29. Copyright 1998 American Association for the Advancement of Science.

electronic structure and ultrafast electron dynamics.[39,207]

On adsorbate-covered surfaces, the IP is modified by the dielectric properties of the molecular overlayer.[42] The IP state series can be further modified through the hybridization with states of the molecular overlayer of the appropriate symmetry.[212] Dependent upon the electron affinity and polarizability of the overlayer molecules, the CB minimum of the overlayer can either be above or below the $n = 1$ IP state. For the negative electron affinity materials such as Ar, the CB is above the vacuum level of the metal; therefore, the bound or quasi-bound states can only exist at the metal−dielectric or dielectric−vacuum interfaces but not in the adsorbate overlayer.[40] However, many molecular overlayers have CBs that overlap with the IP-state Rydberg series, leading to strong mixing. The excitation of these interacting states provides convenient means for injecting electrons into the molecular overlayers.[41,42]

Electrons excited to such conduction−IP hybrid states reflect the character of the parent states; namely, they exist as 2D delocalized waves parallel to the surface but are bound by the crystal and IPs normal to the surface. Parallel to the surface, the hybrid states have parabolic dispersions with effective masses that are usually larger than that of a free electron on account of the interaction with the molecular overlayer.[213,214] If the intersite interaction is weak, then the molecular bandwidth is small and the electron mass will be large. Furthermore, the electron mass will increase through the electronic and dipolar polarization of the overlayer.[215] Electron propagating through the molecular layer is accompanied by a polarization cloud associated with the distortion of the molecular system by the excess charge. If the interaction is sufficiently strong, the inertial dipolar response of the solvent can progressively increase the electron mass until it is localized within the molecular overlayer as an electronic wave packet, that is, a polaron.[29] The localization of electrons also can occur in the presence of structural defects, which create local trapping potentials within the otherwise uniform potential of the overlayer.[41]

4.1. Ultrafast Electron Localization

TR-2PP has been used to study electron solvation for a variety of solvent molecule overlayers on metal surfaces including alkanes, alcohols, nitriles, and water.[41,42] At low temperatures, alkanes physisorb in highly ordered self-assembled overlayers on noble metal surfaces. Because of their nonpolar nature and negative electron affinity, their interactions with excess electrons are relatively weak. Both factors facilitate the direct observation of the dynamical collapse of a delocalized electron wave into a localized wave packet through self-trapping by the solvent (small polaron formation). The studies by Ge at al. on the solvation in self-assembled *n*-heptane monolayers on Ag(111) provide a textbook example of the physics of polaron formation.[29,213]

TR-2PP studies have been performed on ordered *n*-heptane films grown to a monolayer-defined thickness by vacuum deposition onto a Ag(111) surface.[29,213] The 2PP spectra of the heptane-covered Ag(111) surface excited by 4.1 eV of light are dominated by the $n = 1$ IP state associated with the heptane−vacuum interface (Figure 6). Because of its negative electron affinity, its CB of *n*-heptane is above the vacuum level of the Ag(111) surface and the IP states exist mainly at the heptane/vacuum interface. The IP state electron wave functions penetrate into the molecular overlayer only as attenuated evanescent waves. Because of this weak interaction with the molecular film, the IP state on *n*-heptane/Ag(111) surface disperses with $m_{eff} = 1.2m_e$ (Figure 6). Furthermore, because the IP state exists within the ⟨111⟩ projected band gap of silver, the decay of the $n = 1$ IP state electrons by the elastic resonant tunneling into the metal substrate cannot occur for a range of momenta about $k_{||} = 0$.[39] Because of the band gap, electrons transiently excited to the IP state can only decay into the bulk by energy and momentum scattering processes. Therefore, the lifetime of the $n = 1$ IP state is sufficiently long for the dynamical

trapping of electrons by the inertial response of the solvent.[29,213]

Two-color pump−probe measurements of the $n = 1$ IP state presented in Figure 6 reveal the process of electron localization through polaron formation. When the pump and probe pulses coincide in time at zero delay, the 2PP spectra reveal the free-electron-like dispersion of the IP state (Figure 6b). However, when the probe pulse is delayed by 1670 fs, the 2PP spectra are dominated by a nondispersive feature ≤ 10 meV below the dispersive band at $k_{||} = 0$, while the dispersive component is nearly completely attenuated (Figure 6c). This component portends a spatially localized electron wave packet for which the surface parallel momentum is undefined. Pump−probe measurements monitoring the rise of the signal from the localized state for different values of $k_{||}$ were used to map out the process of the wave function collapse in polaron formation.[29,213]

Ge at al. interpreted the dynamics of polaron formation on heptane/Ag(111) surfaces in terms of the inertial response of the solvent to the excess charge.[29,213] In their model, heptane molecules are physisorbed flat, with their C−C bonds parallel to the surface. When excess electrons are injected into the IP state, they induce the polarization of the molecular overlayer. The fluctuations of the molecular internal vibrations in the presence of the excess electron establish a trapping potential, which causes the delocalized wave function to collapse. Ge et al. model the polaron formation dynamics in terms of the excitation of the methylene rocking modes of the adsorbates.[29,213] The free energy of the system is reduced by the electronic and dipolar polarization of the film at the cost of reorganization and electron localization energy. The intensity profile of the localized state as a function of $k_{||}$ gives an estimate of the parallel momentum uncertainty, which has been analyzed theoretically to extract the spatial extent electron localization.[216,217]

The example of electron localization at the heptane/Ag(111) surface provides a window into the dynamics that are likely to cause 2D electron solvation in other molecular systems. However, for other molecular overlayers, either the poor ordering of the overlayer, which creates additional static trapping potentials, or stronger and faster solvent response makes it difficult to resolve the localization process as clearly as the heptane/Ag(111) system.[42]

4.2. Electron Solvation in the Crystalline and Amorphous D_2O Ice

The electron solvation dynamics in water overlayers on metal surfaces studied by Wolf, Bovensiepen, and co-workers[30,41,43,58−60,63,216,218] provide an important counterpoint for related dynamics on metal oxides. On metal surfaces, the solvation dynamics are governed by the degree of crystallinity of ice and the electronic structure of the substrate. The dynamics that can be observed by TR-2PP, such as electron injection, localization, and RCT, which are represented schematically in Figure 7, mainly depend upon the properties of component materials. However, the specific adsorbate−substrate interactions at the H_2O−metal interface beyond the effect on the growth mode of the H_2O overlayer do not appear to be expressed very strongly in the time-resolved experiments on electron solvation in water overlayers on metals.

Bovensiepen and co-workers have performed extensive femtosecond TR-2PP studies of electron solvation in crystalline and amorphous D_2O ice on Ru(001) and Cu(111) surfaces.[30,41,58−60,63] The dynamics are significantly affected by both the nature of the substrate and the crystalline order of ice. It appears that in crystalline ice the strong intermolecular forces that fix the position of molecules at their lattice sites inhibit the fast molecular reorganization that is necessary for effective electron solvation. In ordered overlayers, electrons are solvated mainly at the pre-existing defect sites. In contrast, amorphous ice presents a highly corrugated potential landscape containing many pre-existing trapping sites. Moreover, undercoordinated molecules have sufficient motional freedom[156] to initiate electron solvation on the femtosecond time scale. The dipolar interactions between water molecules and excess electrons are considerably stronger than for the alkane films, leading to a faster solvent response and more significant electron stabilization.

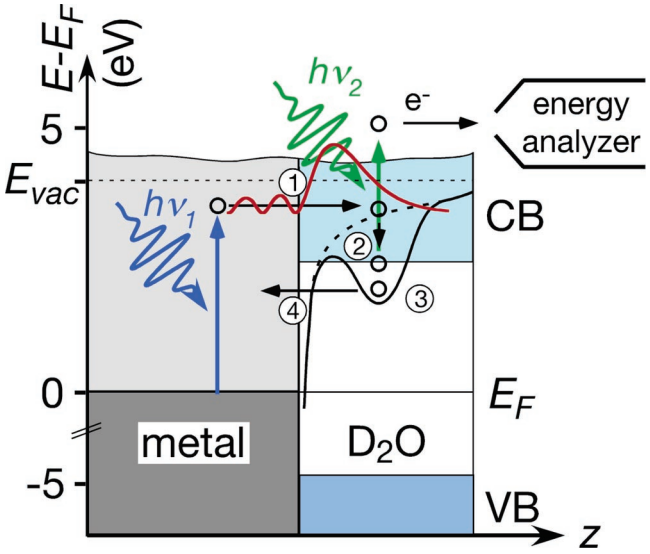

Figure 7. Dynamical processes in two-photon photoemission for D_2O-covered metal surfaces via presolvated electron intermediate states.[41] The photoexcitation with the UV pump laser occurs from bulk states in the metal to IP-D_2O CB hybridized state (red line) of the overlayer (1). Initially delocalized electrons (2) in the CB of ice are localized (3) through the static and dynamical fluctuations of the solvent potential and solvated through the solvent reorganization. RCT into the CB of the metal substrate removes the electron population in competition with energy stabilization through solvation (4). The dynamics are recorded in an energy, momentum, and time-resolved manner by recording the photoemission signal induced by a delayed visible probe pulse.

4.2.1. Electron Solvation in the Crystalline Ice on Metals

The epitaxial relationship between the Ru(001) surface and I_h ice makes it possible to exploit different molecular-film growth conditions to study and contrast the electron solvation in amorphous or crystalline ice on the same surface.[41,60] D_2O deposited on metal surfaces at low temperature (e.g., 135 K) forms amorphous overlayers, which are locally ordered but lack the long-range order of crystalline ice. Such films are characterized by a higher density of H atom acceptor sites and a more porous structure than the crystalline ice.[58] These defects arise because the mobility of water molecules, which is necessary for the bilayer-by-bilayer growth, is suppressed at low temperatures.[26] Highly defective films contain many dangling H/D atom sites that would be consumed by HBs in a perfect crystalline lattice of ice. Both the lack of long-range order and local trapping potentials at

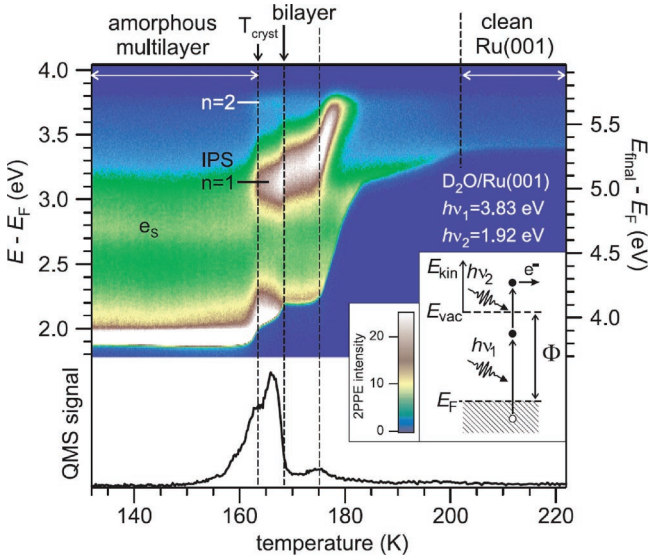

Figure 8. Progressive record of 2PP spectra taken by ramping up the temperature of a D_2O multilayer on Ru(001) from the deposition rate of 135 K to the final temperature of >220 K at a constant rate of 3 K/min. The main changes reflect the amorphous to crystalline phase transition, the desorption of the multilayer to a single bilayer, and the desorption of the first bilayer, as explained in the text and ref 60. e_S represents the presolvated electron feature, and IPS indicates the $n = 1$ and 2 IP states. Reprinted with permission from ref 60. Copyright 2005 Elsevier.

H atom acceptor sites hinder electrons from delocalizing in amorphous ice films.

The effect of the crystalline order on the electronic structure of ice overlayers on metal surfaces is evident in temperature-dependent 2PP measurements performed on a D_2O/Ru(001) sample and presented in Figure 8.[60] In this experiment, D_2O molecules were deposited at 135 K to form an amorphous ice multilayer and the sample was heated progressively while recording 2PP spectra. Initially, the spectra are characteristic of amorphous ice, but at 163 K, the D_2O molecules become sufficiently mobile to recrystallize in a multiple bilayer crystalline phase. The annealing process results in a dramatic change in the appearance of the spectra, which is mainly associated with the appearance of the $n = 1$ IP state for the crystalline phase. Further heating to 166 K leads to the desorption of the multilayer water, leaving only the first bilayer. This is accompanied by an upward shift in the vacuum level and a consequent shift in the IP state energy. The first bilayer, which is more strongly bound than the subsequent bilayers, desorbs at 175 K. Thus, careful control over the annealing conditions can be used to control the ordering and thickness of ice films.[60]

2PP spectra of the annealed D_2O/Ru(001) surfaces excited with a sequence of ~4 eV pump and 2 eV probe pulses reveal the nature of the unoccupied states on water-covered metal surfaces (Figure 9).[60] The spectra of crystalline ice exhibit a prominent peak at 3.15 eV, which is assigned to the $n = 1$ IP state. Unlike for *n*-heptane described above, the CB of water is resonant and, therefore, hybridizes with the IP state of metals such as Ru and Cu. The IP states disperse with an effective mass of $1.3m_e$ as a consequence of the long-range order and periodicity of the crystalline overlayer.[214] They provide the transition moment for the efficient resonant charge transfer from the metal substrate to the molecular overlayer (Figure 7). However, the IP state electrons are delocalized within the overlayer parallel and normal to the surface and, therefore, can efficiently couple

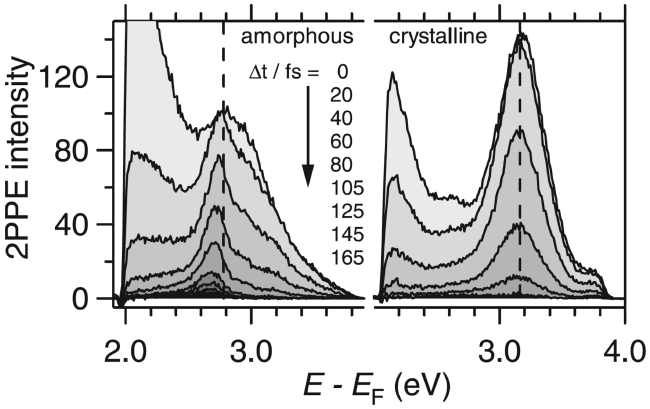

Figure 9. 2PP spectra of amorphous and crystalline D_2O ice on the Ru(001) surface from ref 60. The main feature in the amorphous ice spectrum at 2.9 eV (0 fs delay) indicated by the dashed line is attributed to presolvated electrons (e_s). The peak maximum shifts to a lower energy with delay on account of progressive solvation. The spectra for crystalline ice are dominated by the $n = 1$ IP state at 3.15 eV (- - -), which does not shift and decays considerably faster than e_s. Reprinted with permission from ref 60. Copyright 2005 Elsevier.

to the metal substrate. Consequently, the $n = 1$ IP state electrons decay by RCT into the substrate faster than the experimental time resolution (<5 fs; Figure 10).[60]

It is interesting to note that for properly annealed crystalline ice no features can be attributed to electrons solvated at the water/vacuum interface. Because the IP electrons have a significant probability density at this interface, they could interact strongly with the dangling surface D atoms, as predicted by theory.[149,150] However, the coupling of the IP state to the metal surface is apparently sufficiently strong to effectively compete with the inertial response of the solvent, which occurs through molecular libration on the ~50 fs time scale.[5]

However, the crystalline ice phase also traps a significantly more stable population of solvated electrons, which can persist on minute and longer time scales. These electrons build up over many cycles of laser excitation and have a time- and temperature-dependent peak energy that spans the 0.5−2.0 eV range. The particular stability of these electrons has been attributed to their injection into pre-existing defect sites in the D_2O ice. Their energy and relaxation rates strongly depend upon the ice temperature. At low temperature, the diffusive motion of D_2O molecules in ice is frozen; therefore, the relaxation of the host defect sites is extremely slow. At higher temperatures, diffusion is accelerated, leading to a faster decay of the defect-trapped electrons.[43, 214]

4.2.2. Electron Solvation in the Amorphous Ice on Metals

The significantly more porous and corrugated structure of amorphous ice presents many dangling H atom sites that are not present in the bulk crystalline ice. These broken HBs act as local electron-trapping sites, which strongly modulate the potential experienced by electrons injected into the D_2O overlayer. The same random modulation of the surface potential also affects the energy of IP states. Consequently, there are no distinct features attributable to IP states in the 2PP spectra of the amorphous ice.[41,59,60]

The 2PP spectra of the amorphous ice on Cu(111), Ag(111),[219] and Ru(001) surfaces are characterized by a feature that appears at 2.8 eV for Ru(001) and 2.9 eV for Cu(111) and Ag(111) for normal emission and zero pump−

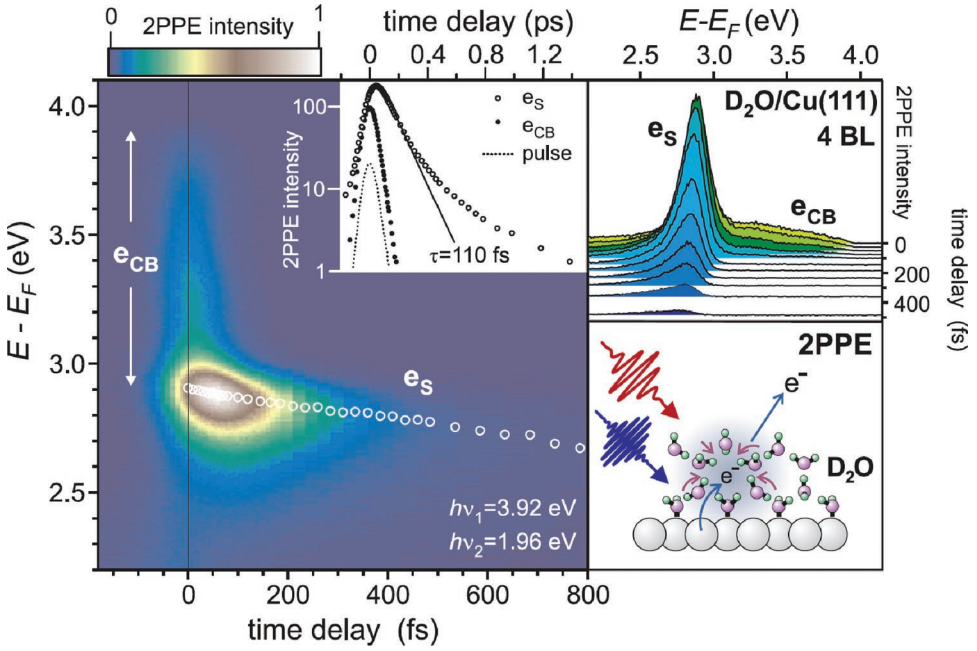

Figure 10. Three-dimensional plot constructed of 2PP spectra at different pump−probe delays showing the e_{CB} and e_s features for D_2O/Cu(111) from refs 41 and 59. The upper right inset shows individual spectra for different delays used in the construction of the 3D plot. The center inset shows the decay kinetics measured separately for the e_{CB} and e_s populations. The e_s feature corresponds to electrons trapped at static and dynamical potential fluctuations associated mainly with the dangling D acceptor atoms (lower right inset). Reprinted with permission from ref 41. Copyright 2005 Elsevier.

probe delay.[58,60,219] At later delays or for $k_{||} \neq 0$, this feature can be weakly resolved into two components. The first, weaker component (e_{CB}) corresponds to delocalized electrons at the CB minimum. The e_{CB} electrons exhibit positive dispersion with an effective mass of 1.0 (0.2)m_e, indicating a high degree of delocalization, and decay within the duration of the laser pulse (<70 fs).[59] The narrower and more intense feature (e_s) corresponds to trapped electrons initially at the CB minimum. The e_s feature exhibits apparent negative dispersion ($m_{eff} < 0$), which Bovensiepen and co-workers attributed to the localization of presolvated electrons.[59] The e_s electrons have significantly longer lifetimes than the e_{CB} electrons, and their energy decreases with the pump−probe delay. The longer lifetime and energy stabilization are indicative of progressive solvation by the D_2O overlayer, as indicated schematically in Figure 7.[30,58] Both the e_{CB} and e_s features probably derive some of their oscillator strength through the hybridization with the inhomogeneously broadened IP states.

As in the crystalline ice, the e_{CB} electrons are delocalized and mobile, allowing them to couple strongly with the substrate. Consequently, they decay on the <10 fs time scale either through RCT or by solvation to the e_s form. The longer lifetime of e_s electrons provides information on the changes of their solvation environment with the delay time. Besides the energy stabilization, the increasing degree of solvation of e_s electrons increases the curvature of their negative dispersion and the angular width of their photoemission distribution.[59,63,216] The parallel momentum width $\Delta k_{||}$ of the e_s emission peak provides information on the spatial extent of solvated electrons Δx according to the approximate relation $\Delta x \sim 1/\Delta k_{||}$.[30] The spatial extent of electrons derived from the $k_{||}$ distribution of 15−25 Å is consistent with estimates of electron localization from the geminate recombination in the bulk water.[30,59,133] Andrianov et al. have extended the analysis of Harris and co-workers on the effect of localization on 2PP angular distributions to obtain more quantitative estimates of the progressive electron localization for the D_2O/Cu(111) system.[42,56,216]

Further information on the dynamics at the CB minimum has been obtained in a higher temporal resolution study (10 fs) of Bovensiepen et al. on H_2O/Cu(111). When 3.1 eV photon energy pump and probe pulses are employed, the e_s feature could be studied without significantly exciting the e_{CB} electrons.[218] These experiments reveal that electrons initially injected at 2.97 eV decay within 30 fs to 2.85 eV.[30] These time and energy scales for this rapid energy relaxation process correspond well to the inertial libration of water. Thus, electrons at the CB minimum appear to be solvated by the reorientation of water molecules, which create a trapping potential within the porous structure of amorphous ice.

After electrons are trapped at the CB minimum, it is possible to follow the energy and population evolution of the e_s feature for ~1 ps (Figure 10). After the initial energy relaxation process observed in 10 fs resolution experiments, the energy and population decay of e_s occurs in a biexponential manner that depends upon the substrate and overlayer thickness.[58,63] For <2 BL D_2O thickness on Cu(111), the energy and population relaxation are significantly more rapid than for thicker films. The e_s peak shift occurs at a rate of ~1 eV/ps.[58] At low coverages, the surface is not fully covered by amorphous ice and the reorganization of water molecules is less constrained by intermolecular interactions. Therefore, both RCT and solvation can proceed more rapidly than at higher coverages.

For fully covered Cu(111) and Ru(001) surfaces (>2 BL), the apparent energy relaxation proceeds initially at rates of 270 and 830 meV/ps, respectively.[63] The population decay integrated over the evolving e_s energy distribution occurs in a biexponential manner (Figure 11). The fast components of 140 and 34 fs for the Cu(111) and Ru(001) surfaces, respectively, strongly depend upon the substrate, while the slow components of ~300 fs are nearly substrate-indepen-

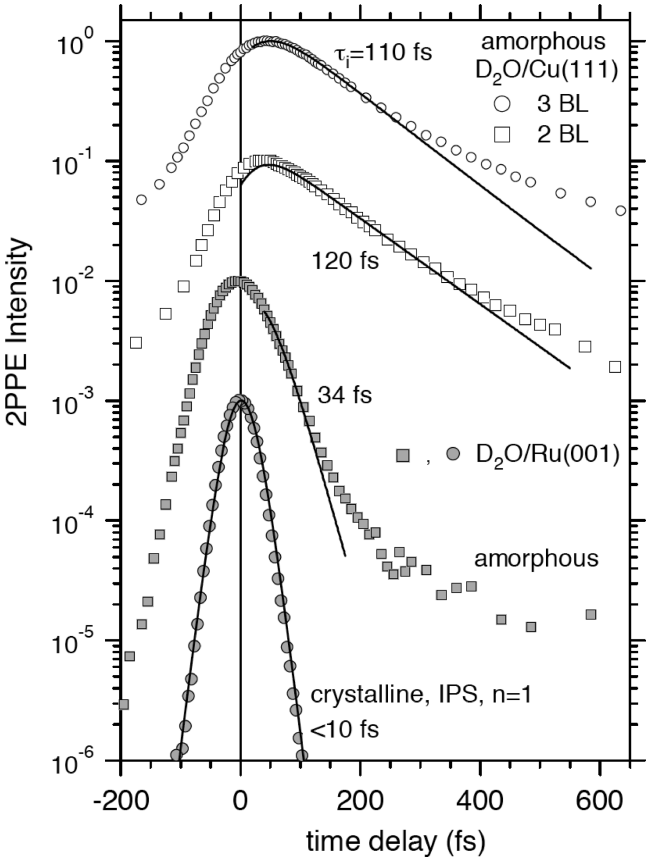

Figure 11. Characteristic pump−probe measurements of the decay of e_s and IP $n = 1$ features for D_2O/Cu(111) and D_2O/Ru(001) (amorphous and crystalline). Reprinted with permission from ref 41. Copyright 2005 Elsevier.

dent. The initial dynamics clearly include the interaction of presolvated electrons in the D_2O overlayer with the metal substrate, which leads to a rapid decay by RCT, in addition to the energy relaxation through progressive solvation. At later times, when electrons are more fully localized, the dynamics become more representative of the molecular overlayer. The RCT rates depend upon the density of states (DOS) of the substrate and the presence of projected band gaps.[209] Stähler et al. attribute the faster initial decay on the Ru(001) surface to the latter effect,[63] because the energetic edge of the accepting bulk band is closer (1.5 eV above E_F versus 0.9 eV below E_F) to the CB minimum of D_2O than for Cu(111). Because of the proximity to the band edge, the range of $k_{||}$ states available for the decay into the substrate is therefore larger for the Ru(001) surface.

At longer times, RCT is substrate-independent because its rate is dominated by the tunneling through a solvent-imposed barrier that does not strongly depend upon the electronic structure of the substrate. After the contribution of RCT to the decay traces was taken into account, Stähler et al. obtained the actual energy relaxation rates of 0.24 and 0.22 eV/ps for Ru and Cu, respectively. The comparable energy relaxation rates indicate that electrons on Ru and Cu substrates exist and evolve in similar molecular environments. The much faster and substrate-dependent effective energy relaxation rates result from the differences in the electronic structures and the energetic barriers (2.77 eV for Ru versus 2.93 eV for Cu), which determine the RCT rates into the substrates. The higher RCT rates near and above the energetic barriers preferentially remove the less solvated, higher energy electrons from the distribution.[63]

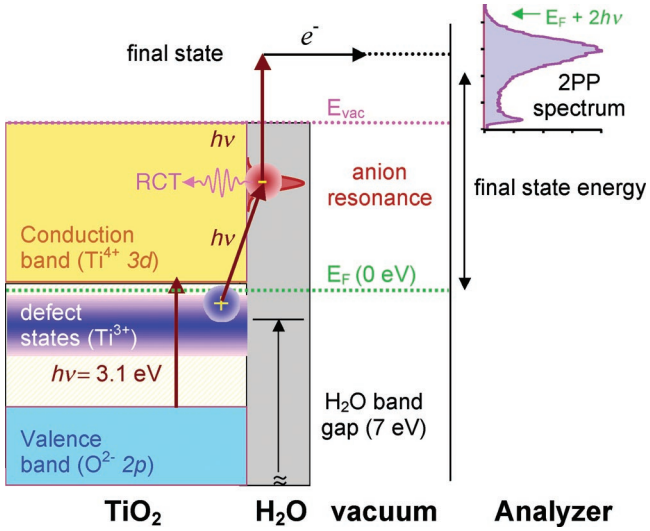

Figure 12. Schematic diagram for 2PP excitation at H_2O-covered reduced TiO_2(110) surfaces. The primary process of interest is the charge-transfer excitation from the defect band into the H_2O overlayer. Assuming no excitonic interaction between the electron and its hole, the excitation creates a transient anionic state of the overlayer. Further excitation above the vacuum level (E_{vac}) emits electrons from the H_2O overlayer into the vacuum. The wet electron state decays by the RCT into the CB of TiO_2.

5. Electron Solvation in Molecular Overlayers on Metal Oxide Surfaces

Although the electronic properties of water on metals are of fundamental interest, the water/metal oxide interface is of much greater practical significance. However, in comparison to metals, much less is known of the electron solvation in molecular overlayers on metal oxides. As discussed in section 3.2, each metal oxide provides a different template for the adsorption of molecular overlayers. Moreover, even for surfaces with similar structure, the acid/base character of the surface can have a strong effect on whether the molecules adsorb associatively or dissociatively. Thus, specific interactions between the adsorbate and substrate in the first and perhaps several subsequent monolayers can have a strong influence on the interfacial electronic structure and charge-transfer dynamics on metal oxide surfaces.

5.1. Electronic Structure of TiO_2(110) Surfaces

The electron interaction with hydrous overlayers on the rutile TiO_2(110) surface has been investigated because of interest in the application of TiO_2 nanocolloids in photocatalytic processes, such as splitting of H_2O into H_2 and O_2, and photovoltaic solar energy conversion.[65,66,220−224] The electronic structure of TiO_2(110) surfaces, which is central to the understanding of these processes, has been studied extensively by photoemission, inverse photoemission, and 2PP spectroscopy.[225−229] The valence and conduction bands of TiO_2 are derived, respectively, from the O 2p and Ti 3d states. For the rutile and anatase polymorphs, they are separated by band gaps of 3.05 (Figure 12) and 3.2 eV.[230] TiO_2 is easily reduced either by the generation of O atom vacancy defects or by chemisorption of electron-donating adsorbates. Upon reduction, a defect band forms 0.1 eV below the CB minimum with a maximum DOS appearing 0.9 eV below E_F (Figure 12).[160,225,231]

TiO_2(110) surfaces have a characteristic structure of bridging O_b atom rows along the [00$\bar{1}$] crystallographic

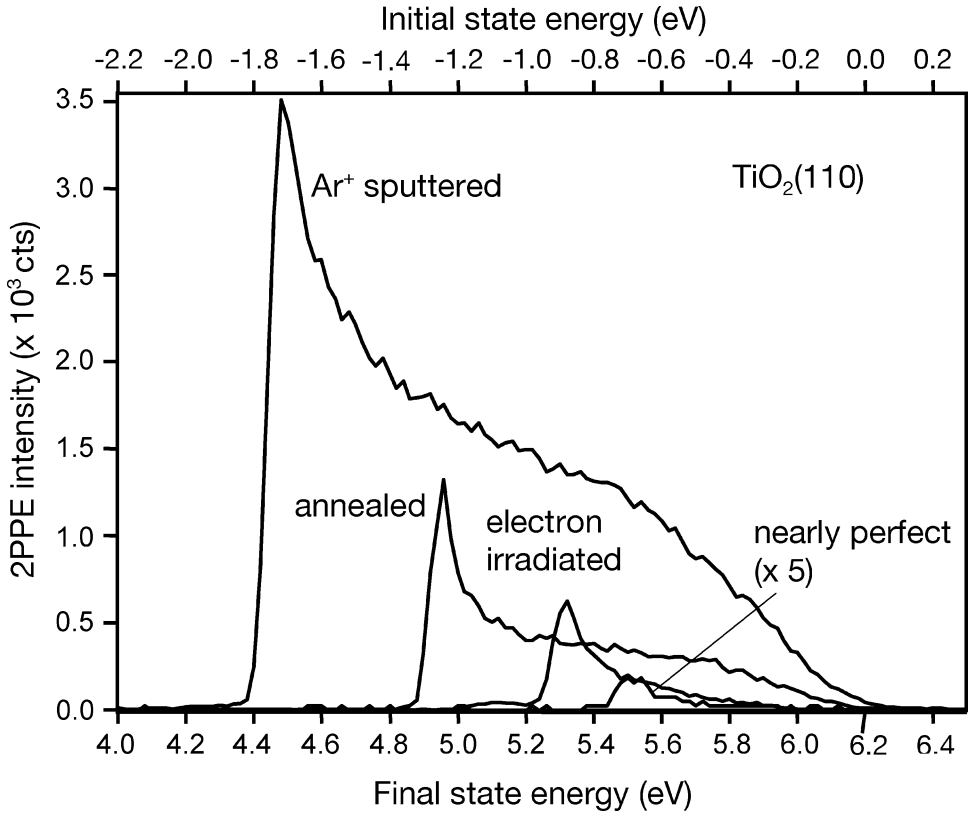

Figure 13. Characteristic 2PP spectra of the TiO_2(110) surface after different preparation protocols from ref 228. The vacuum level edge shifts to a lower energy, and the defect state-derived intensity increases with the degree of surface reduction. Reprinted with permission from ref 228 (http://link.aps.org/abstract/PRB/v70/p045415). Copyright 2004 American Physical Society.

direction and five-coordinate Ti_{5c}^{4+} ions in troughs between the O_b rows (Figure 5a). The surface is well-known for its propensity to form bridging O_b atom vacancy defects, which are highly reactive toward the dissociation of molecular adsorbates. The dissociation products, which are strongly chemisorbed,[191] can participate in the electron solvation and interfacial charge-transfer processes.

The concentration of the O_b atom defects can be controlled by the surface preparation methods. Sputtering followed by annealing of TiO_2(110) in O_2 atmosphere at 900 K produces surfaces that are nearly stoichiometric.[195] O_b atom vacancy defects can be introduced with a different degree of control by subsequent irradiation with high-energy electrons (500 V), annealing at high temperatures (>900 K) in a vacuum, or sputtering with energetic ions.[228] The most commonly used procedure of vacuum annealing removes approximately 5% of the bridging O atoms, creating O_b vacancy defects.[195]

For each O_b atom removed, two excess electrons remain on the surface. These electrons are transferred to the above-mentioned shallow defect band and delocalize over several sites in the unoccupied d orbitals of the surface Ti_{5c}^{4+} ions.[232,233] The defect band can also be occupied by reducing TiO_2 surfaces through chemisorption of H atoms, alkali atoms, and even electron-donating molecules such as H_2O and CH_3OH.[186,228,234]

The surface preparation protocol has a strong influence on the 2PP spectra of TiO_2(110) surfaces.[62,228] Figure 13 shows 2PP spectra of nearly perfect, electron-irradiated, vacuum-annealed, and Ar^+-sputtered TiO_2(110) surfaces excited with 3.1 eV photons.[228] The spectra of surfaces with an increasing degree of reduction show a progressive increase in the overall emission intensity and a decrease in the work function. Although, the 3.1 eV photon energy is sufficient to excite electron−hole (e−h) pairs across the band gap of TiO_2, it cannot complete the 2PP process by further exciting electrons above the work function (Figure 12). 2PP with 3.1 eV photons can only be excited from the shallow defect states that exist as a consequence of the surface reduction.

The increase in intensity of 2PP emission and the decrease in the work function of TiO_2 in Figure 13 correlate with the degree of reduction of the surface. Removing the electronegative O atoms decreases the work required to transport electrons from TiO_2 into vacuum. Therefore, the work function is sensitive to the defect concentration on TiO_2 surfaces.[228] Surfaces with low work functions are likely to have a large concentration of defects or adsorbed impurities, which can strongly affect the interfacial charge-transfer dynamics. The 2PP spectra of the nearly perfect, that is, stoichiometric surface in Figure 13 has a nearly vanishing intensity of the defect DOS and the highest work function. This is consistent with the minimal occupation of the defect band and, therefore, the lowest degree of surface reduction. Repeated measurements on different samples give a consistent value of 5.6 (1) eV for the work function of the stoichiometric TiO_2(110) surfaces.[228]

The 2PP spectra of TiO_2(110) surfaces in Figure 13 also differ in their intensity, which is related to the degree of the surface reduction. The spectra reveal no distinct spectral features, and time-resolved measurements indicate that the intermediate states in the 2PP process have a lifetime of $\ll$10 fs. The short effective lifetimes imply either that the electronic relaxation of the intermediate states occurs through processes such as e−e scattering on extremely fast time scales or, more likely, that the 2PP process occurs through virtual intermediate states.[228,235] Even though 2PP excitation from the valence band to a level 0.8 eV above E_F in the CB

has been reported for excitation with ~4.5 eV photons,[229] the 2PP process from the defect band excited with 3.1 eV photons does not appear to be enhanced by resonant excitation of intermediate states in the CB of TiO_2. This is consistent with the optical absorption and electron energy loss spectra of reduced TiO_2 surfaces.[236,237] Thus, the increasing intensity of 2PP spectra in Figure 13 as a function of surface reduction reflects mainly the increasing occupation of the defect band.

5.2. Wet Electrons on H/H_2O/TiO_2(110) Surfaces

5.2.1. Occupied Electronic Structure of H_2O/TiO_2 Surfaces

The electronic structure of H_2O on TiO_2 has been studied extensively by UV photoelectron spectroscopy (UPS) and X-ray photoelectron spectroscopy (XPS).[196,202,204,225] Low-coverage UPS spectra show features arising from the defect-mediated dissociation, which leads to the formation of surface −OH, while at higher coverages, molecular chemisorption dominates. The highest occupied $1b_1$ lone-pair nonbonding orbital of H_2O on TiO_2 appears 7.7 eV below E_F, while the π orbital of surface −OH is 8.0 eV below E_F.[196,225] Because the optical band gap of free water molecules is ~7 eV, the 3.1 eV of light cannot excite transitions within H_2O molecules. Moreover, the photoemission spectra of chemisorbed water on TiO_2 resemble those of H_2O liquid jets.[238] Assuming that the vacuum level of H_2O liquid jets corresponds to the CB of H_2O on TiO_2, than the binding energy of the $1b_1$ orbital of 11.16 eV observed for H_2O liquid jets[238] places the CB of H_2O on TiO_2 at 3.5 eV above E_F.

5.2.2. Unoccupied Electronic Structure of H_2O/TiO_2 Surfaces

The chemisorption of ~1 ML of H_2O on the stoichiometric TiO_2 surfaces produces changes in the 2PP spectra (Figure 14a) that can be mainly attributed to the charge transfer from the molecular overlayer to the substrate.[62] Chemisorption of H_2O substantially lowers the work function of the TiO_2 surface and increases the characteristic DOS of the defect band. Both changes are consistent with partial charge transfer from the molecular overlayer to the Ti 3d states at the CB minimum of the substrate. The decrease of the work function with the H_2O coverage has been simulated with the Helmholtz model to deduce an effective dipole moment of 0.5 D for the chemisorbed H_2O.[228] This magnitude of dipole moment is comparable to that for the chemisorption of H_2O on metals.[228] Significantly, the 2PP spectra of stoichiometric H_2O/TiO_2 surfaces excited with 3.1 eV of light (Figure 14a) exhibit no additional features, such as observed for metals, that could be assigned to the injection of electrons into the CB of H_2O.[62] This is consistent with the aforementioned energy of 3.5 eV for the CB of H_2O overlayers.

By contrast to stoichiometric surfaces, the chemisorption of H_2O on the reduced TiO_2(110) surfaces leads to a new spectroscopic feature that can be attributed to an unoccupied state 2.4 eV above E_F.[62,228] In Figure 14b, this feature appears only with p-polarized excitation light, indicating that the transition moment is normal to the surface. In the difference spectrum between 2PP spectra excited with p- and s-polarized light, the unoccupied resonance has the characteristic asymmetric line shape already encountered in other spectra of solvated electrons. Because it is absent in the spectra of clean TiO_2 surfaces and H_2O on the stoichiometric TiO_2 surfaces, this spectrum cannot be attributed to the excitation entirely within TiO_2 or TiO_2 covered by intact H_2O molecules.

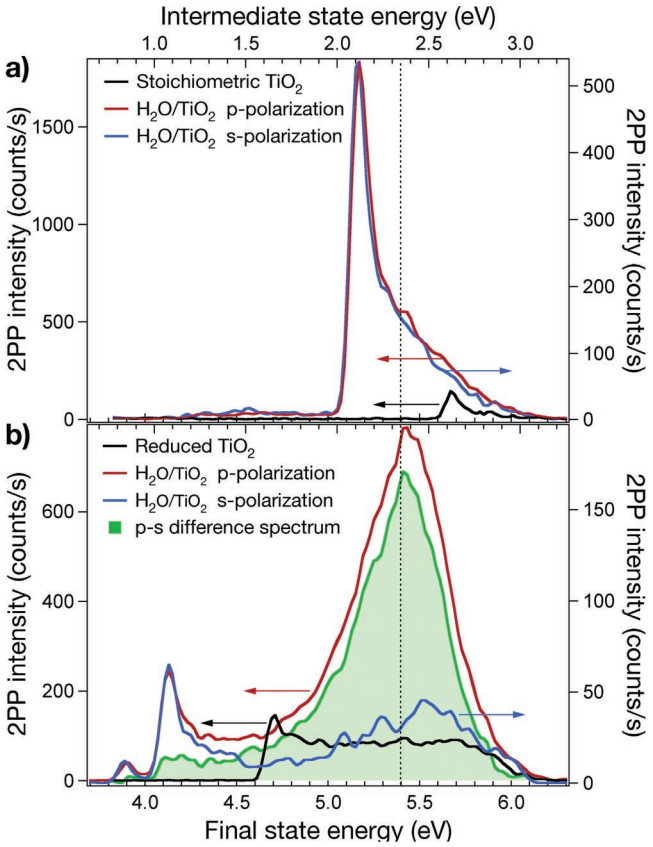

Figure 14. 2PP spectra of the (a) stoichiometric and (b) reduced TiO_2(110) surfaces before and after adsorption of 1 ML H_2O from ref 62. The spectra are recorded with s- and p-polarized excitation and are normalized at ~4.1 eV. The difference spectrum (green) shows the wet electron resonance for the reduced H_2O/TiO_2 surface. The dotted line indicates the energy of the wet electron resonance.

The 2.4 eV peak in Figure 14b has been assigned to the partially solvated or "wet" electrons associated with the dangling H acceptor atoms of surface −OH and H_2O based on evidence from chemical, spectroscopic, and theoretical studies.[62] The spectrum only appears on reduced TiO_2 surfaces, where the dissociation of H_2O at O_b vacancy defect sites leads to the formation of minority surface −OH species. However, the appearance of the wet electron resonance also requires the presence of majority H_2O species.

The wet electron resonance shows a characteristic dependence on the H_2O coverage. Figure 15 shows a series of 2PP spectra after exposing a vacuum-annealed reduced TiO_2 surface to different amounts of H_2O. The wet electron resonance intensity rises to reach the maximum as the H_2O coverage is increased to approximately 1 ML coverage. The coverage can be calibrated by either the dependence of the 2PP spectra on the surface temperature, which takes advantage of the large difference in desorption temperatures between the first and second monolayers, or the work function change.[62] For coverages above 1 ML, the resonance intensity is diminished and saturates at ~25% of its maximum value.[62] The strong coverage dependence of the resonance intensity indicates that the carrier of the spectrum has a pronounced interfacial character, which is most strongly expressed at 1 ML coverage. The 2PP spectra in Figures 14 and 15 indicate that the wet electron resonance is observed when both the minority surface-bound −OH and majority 1 ML chemisorbed H_2O are present on TiO_2 surfaces.

The assignment of the resonance to minority −OH and majority H_2O species can be confirmed by an alternative

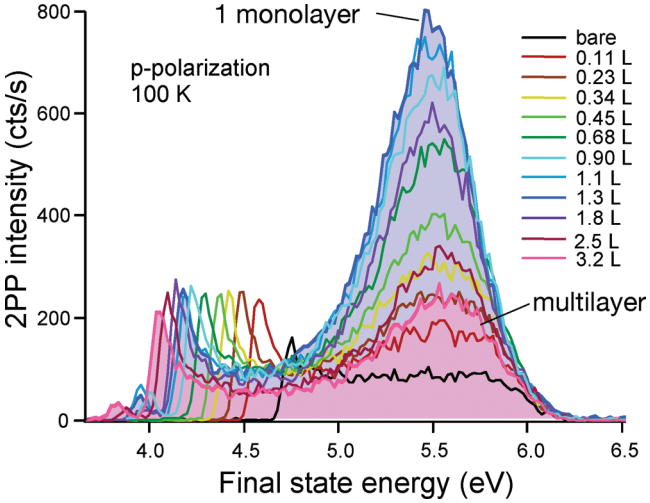

Figure 15. Series of consecutive spectra after exposure of a reduced TiO_2 surface to increasing amounts (in Langmuir) of H_2O.[61] Blue- and red-highlighted spectra represent the 1 ML intensity maximum and multilayer saturation limits, respectively.

protocol for the preparation of reduced TiO_2 surfaces. Figure 16 shows a series of 2PP spectra where the stoichiometric TiO_2 surface is exposed to a diffusive source of H atoms, which is followed by various exposures to H_2O.[239] Whether surface −OH is formed by the dissociation of H_2O or the adsorption of H atoms, the same resonance at 2.4 eV appears in 2PP spectra after deposition of ∼1 ML of H_2O. This alternative preparation method confirms the joint role of surface −OH and H_2O species as the carriers of the wet electron spectrum.

The wet electron resonance has been assigned on the basis of the DFT calculation of the unoccupied structure of H- and H_2O-covered TiO_2(110) surfaces.[186] The calculations were performed for different H and H_2O coverages and H_2O chemisorption structures. The conclusions are not strongly dependent upon specific details of coverage and structure; therefore, Figure 17 presents only the molecular and electronic structure of the 0.5 ML H- and 1 ML H_2O-covered TiO_2(110) surface, which is the most relevant structure for interpreting the experimental results. At 0.5 ML coverage, H atoms bound to O_b atoms are sufficiently far apart (5.92 Å), not to interact through space, and therefore are representative of experimentally investigated surfaces with sparse −OH coverage.

The structure of the H_2O overlayer in the presence of H atoms is nearly the same as for the pure H_2O overlayer in Figure 5. The additional H atoms on the O_b rows have a surface-normal orientation in the absence of H_2O. Therefore, they do not interact strongly with the nearly surface-parallel H_2O molecules located between the O_b rows. Nevertheless, bending of surface −OH for H_2O-covered surfaces toward the proximate H_2O molecules suggests the formation of a weak HB. However, the H···O length of this HB of 3.07 Å is outside the usual range of bond lengths attributed to HBs[23] and therefore is considerably weaker that the intermolecular and molecule-surface HBs formed by H_2O molecules.

This pattern of hydrogen bonding calculated for the equilibrium ground-state structure for $H/H_2O/TiO_2$ surfaces determines the spatial probability distribution of the unoccupied state orbital. The right side of Figure 17 transposes the excited-state unoccupied orbital distribution on the optimized structure of the $H/H_2O/TiO_2$ surface. The unoccupied DOS of adsorbate-localized states increases from ∼1.5 eV above the CB minimum. The orbital presented in Figure 17 corresponds to the energy where the molecule-projected DOS integrated from the CB minimum equals the DOS of one electron.[186] The energy of this reference orbital at 2.6 eV above the CB minimum is in good agreement with the experimental observation.[62]

Typical of other calculated H- and H_2O-covered surfaces, the unoccupied orbital has the largest density at the bridging −OH species. Additional density of the unoccupied orbital spreads from the −OH species over the H atoms of two proximate H_2O molecules that are involved in the weaker intermolecular HBs. However, the strongest H_2O molecule-surface HBs receive almost no density. Thus, the DFT calculations indicate that the surface −OH species with the aid of weakly hydrogen-bonded H atoms on proximate H_2O molecules stabilize electrons injected into the hydration layer at the $H/H_2O/TiO_2$ surfaces. The electron stabilization is a cooperative effect of surface −OH and H_2O molecules as expected from the 2PP experiments. The calculated unoccupied states associated with the isolated −OH species, which correspond to the reduced TiO_2 surfaces without the H_2O overlayer, or the pure H_2O overlayer, which correspond to H_2O chemisorbed on stoichiometric TiO_2 surfaces, are too high to observe in 2PP experiments with 3.1 eV photons.[186]

The cooperative interaction between the interfacial dangling H atoms also explains the H_2O molecule coverage dependence of the wet electron resonance. The adsorption

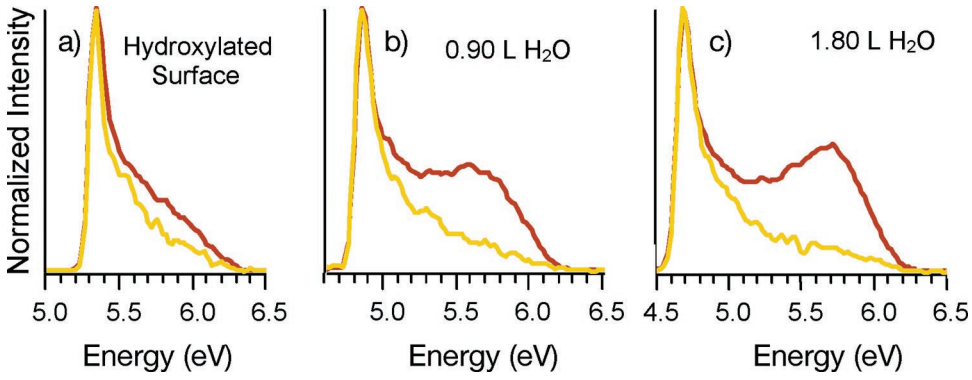

Figure 16. 2PP spectra of TiO_2 surfaces after reduction with an effusive H atom beam for (a) no coadsorbed water and after exposure to (b) 0.90 and (c) 1.80 Langmuir of H_2O at 90 K surface temperature (1.35 L exposure corresponds to approximately one monolayer; 1 ML of H_2O).[62] The spectra are measured with s- and p-polarized excitation light (orange and red, respectively).[239] The excess DOS for p-polarized excitation for H_2O-covered surfaces can be attributed to the wet electron resonance. Some wet electron DOS is also observed even for the hydroxylated surface because of the reaction of H atoms to form H_2O on the UHV chamber surfaces.

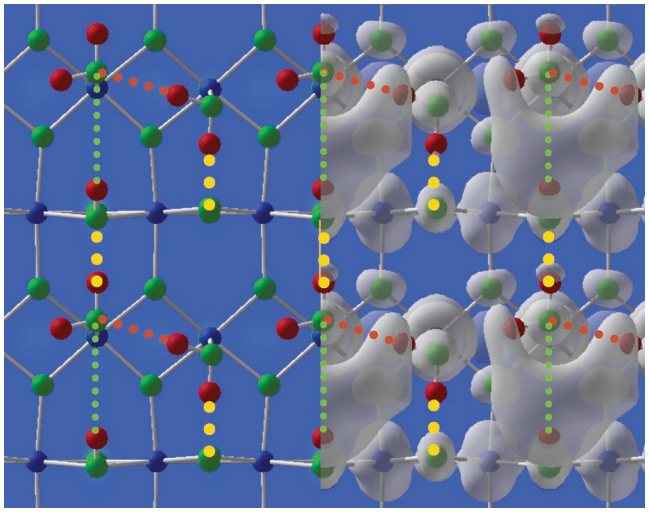

Figure 17. Optimized molecular structure of 0.5 ML H and 1 ML H_2O on the TiO_2(110) surface (left) and the same structure with the unoccupied state probability distribution superimposed on the molecular structure (right).[186] Green, orange, and yellow lines represent hydrogen bonds of increasing strength. The unoccupied DOS is concentrated on H atoms of surface −OH species that form the weakest hydrogen bond. Reprinted with permission from ref 186 (http://link.aps.org/abstract/PRB/v73/p195309). Copyright 2006 American Physical Society.

of the second ML of H_2O molecules disrupts the favorable surface −OH sites that are primarily responsible for the wet electron resonance. Because the first monolayer H_2O molecule H atoms are engaged in favorable HBs, there are few favorable adsorption sites for the second monolayer H_2O molecules.[191,192] In bilayer structures on metals, dangling H atoms in the topmost layer can template the subsequent growth of crystalline H_2O ice. However, the strong H_2O−metal oxide interaction does not favor epitaxial growth of the second monolayer. Even though the TiO_2(110) surface is hydrophilic for the first monolayer, the strong molecule−surface interaction makes the first monolayer surface hydrophobic for the subsequent layers. On $H/H_2O/TiO_2$ surfaces, the minority dangling H atoms of surface −OH are the most favorable sites for the hydrogen bonding of the second ML H_2O molecules. The formation of HBs with the second ML H_2O molecules, thus, removes favorable sites for the stabilization of excess electrons injected into the molecular overlayer and, therefore, reduces the wet electron resonance intensity.

The lack of additional spectroscopic features that could be attributed to the injection of electrons into the CB of the H_2O overlayer is also notable for multilayer H_2O/TiO_2 surfaces. The DFT calculations for the 1 ML H_2O/TiO_2 surface and UPS spectra locate the CB of H_2O 3.5 eV above E_F, which is substantially higher than 2.8−2.9 eV for H_2O on metals.[41] Thus, the excitation to the CB of H_2O on TiO_2 surfaces may require higher photon energy. The excitation into the CB of H_2O overlayers also may be difficult because of a small transition moment. The hybridization of the CB of H_2O with the IP states that appears to be important for the charge-transfer excitation on metals is nonexistent on metal oxides. Moreover, the favorable HB network of the first monolayer H_2O molecules may present a barrier for transmitting electrons between the substrate and the amorphous ice overlayer.

5.2.3. Interfacial Charge-Transfer Dynamics

Considering the electronic properties of TiO_2 surfaces following the reduction with H atoms, we can further define the nature of the wet electron state and charge-transfer dynamics on $H/H_2O/TiO_2$ surfaces. The O_b atoms on the stoichiometric surface have the nominal valence of O^{-2}. H atoms bring an additional electron, which cannot be accommodated by the saturated valence shell of O_b atoms. Therefore, the excess electron is mainly transferred to the 3d defect band on the neighboring Ti_{5c}^{4+} ions, leaving a net positive charge on the H atom.[186,232] In photoexcitation with 3.1 eV photons, an electron is transferred from the Ti 3d defect band to the wet electron orbital localized on the H atoms of the surface −OH species. Thus, the ground and excited states can be thought of as charge-transfer resonance structures.

The large charge displacement between the ground and excited states provides a favorable transition moment for the optical excitation. The excitation occurs nonadiabatically, creating the excited state in the ground-state geometry. Interferometric pump−probe measurements resonant with the wet electron state give a maximum value of its lifetime of ∼15 fs at 1 ML H_2O coverage.[186] The excited state decays most likely by nonadiabatic RCT into the CB of TiO_2 before the nuclear motion of the molecular overlayer can stabilize (solvate) the new charge distribution. The time scale for RCT is faster than the H_2O libration and corresponds to only about two periods of the OH stretching vibration.

5.3. Wet Electrons on $H/CH_3OH/TiO_2$(110) Surfaces

Electron solvation has also been studied in liquid methanol and in methanol overlayers on Ag(111) and TiO_2(110) surfaces.[31,57,61,118,119,126] As discussed in section 2.2.2, because of the direction of its dipole moment and the lower density and frequency of its librational states, the solvation dynamics in liquid methanol are dominated by inertial translation, which is considerably slower than H_2O libration.[122,126,127] For CH_3OH/Ag(111) surfaces, the solvation dynamics appear to be similar to those of amorphous H_2O ice on metals.[57] The initial charge injection into the CH_3OH overlayer occurs via excitation of the IP states. After injection into the IP states at >3 eV, electrons undergo ultrafast (∼200 fs) relaxation by ∼0.2 eV to a presolvated state and, thereafter, decay by RCT with a time constant of ∼250 fs back to the substrate. The solvation dynamics in CH_3OH overlayers on the TiO_2 surface are substantially more complex.[31,61]

5.3.1. Wet Electron States on $H/CH_3OH/TiO_2$(110) Surfaces

The measurements on CH_3OH/TiO_2(110) surfaces provide a much more detailed picture of electron solvation in protic solvents on metal oxide surfaces than the measurements for H_2O/TiO_2 surfaces.[31,61] Just like H_2O, CH_3OH dissociates at O_b vacancy defects upon chemisorption on reduced TiO_2(110) surfaces.[240−242] The dissociative chemisorption incorporates minority −OH and $-OCH_3$ species in the O_b rows. Further chemisorption occurs at the Ti_{5c}^{4+} sites, where according to both experiment and theory, a fraction of the chemisorbed molecules dissociate (deprotonate) to form $-OCH_3$ at the Ti_{5c}^{4+} sites and −OH at the bridging sites.[31,240,242,243] DFT calculations find that the 50% dissociated structure of CH_3OH is more stable than the molecularly

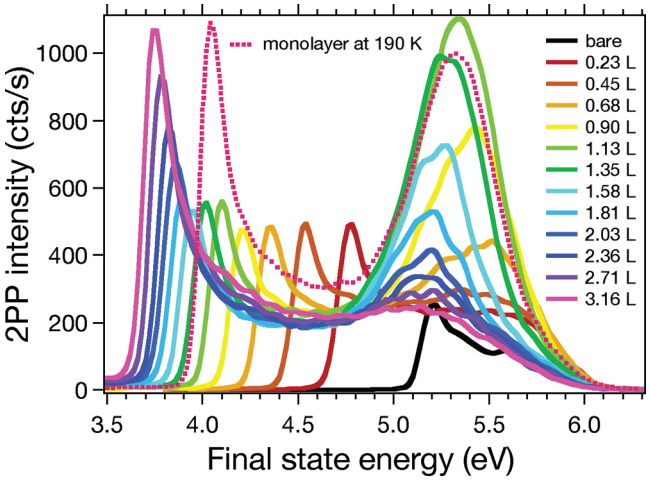

Figure 18. Series of 2PP spectra after progressive exposures of a reduced TiO_2(110) surface to CH_3OH at 100 K. The maximum peak intensity at 1 ML coverage is determined by heating a surface with multilayer coverage to 190 K (···) to remove all but the first monolayer molecules.[61,239]

chemisorbed or fully dissociated strtuctures.[31] The OH of methanol can form favorable HBs with either the substrate O_b atoms or the O atoms of the neighboring CH_3OH molecules. Likewise, the −OH species on the bridging rows can make HBs with the $-OCH_3$ or CH_3OH species at the Ti^{4+}_{5c} sites. With only one strongly electropositive H atom available for hydrogen bonding per CH_3OH molecule, the rutile surface can accommodate all such H atoms of molecularly and dissociatively chemisorbed CH_3OH in favorable HBs.

2PP spectra for different exposures of CH_3OH on the reduced TiO_2 surface are shown in Figure 18. A peak associated with the molecular overlayer appears at submonolayer coverages and evolves through an intensity maximum as the coverage is increased. Simultaneously, the peak position shifts to a lower energy.[61] On the basis of the temperature dependence of 2PP spectra, Onda et al. have established that the exposure of 1.1 Langmuir corresponds to ∼1 ML coverage.[61] At this coverage, the peak 2.3 eV attains the maximum intensity. Above 1 ML coverage, the intensity saturates at approximately 25% of its maximum value. Furthermore, even for the stoichiometric TiO_2 surfaces, the resonance appears with similar properties except for the significantly reduced intensity. Measurements of the resonance dispersion with parallel momentum confirm that the electronic state is localized in the CH_3OH overlayer. Except for the coverage-dependent energy shift, considerably higher intensity, and appearance even for stoichiometric surfaces, the CH_3OH-induced peak has similar spectroscopic properties as the wet electron resonance on H_2O/TiO_2 surfaces, which suggests a related origin.[61] On the basis of these similarities and electronic structure calculations, we attribute the CH_3OH-induced peak to partial surface solvation of excess electrons.[31,186]

5.3.2. Solvation Dynamics on the H/CH_3OH/TiO_2(110) Surfaces

The solvation dynamics of electrons injected into CH_3OH overlayers on TiO_2 are substantially more complex than for H_2O/TiO_2. Figure 19 shows representative 3D plots constructed from pump−probe two-pulse correlation measurements for a range of energies near the CH_3OH resonance for three different CH_3OH coverages. These experiments were performed for both CH_3OH and CH_3OD, with the expectation that the deuterium isotope substitution might elucidate the role of OH species in the electron solvation.

The data in Figure 19 indicate a strong CH_3OH coverage and deuterium isotope effect on the electron solvation and charge-transfer dynamics. At low coverage (<1 ML), the injected electron dynamics can be described by single-exponential kinetics that have a weak dependence on the measurement energy. The individual pump−probe measurements for selected energies in Figure 19a show that the lifetimes on the order of ∼20 fs increase moderately at lower (below the peak maximum) energies. The 3D plots reveal that this weak energy dependence reflects a moderate (∼0.1 eV) peak shift to lower energies at longer pump−probe delays. The excited state is weakly stabilized in energy on a ∼30 fs time scale, as is more evident from higher coverage measurements. However, at low coverage, the population decay is faster than the energy relaxation and the deuterium isotope effect is nearly absent.[31]

At coverages in the range from 1 to <2 ML (Figure 19b), the solvation dynamics become considerably more complex. The high-energy decay (above the resonance) is still single-exponential, but below the resonance, the individual scans show clear evidence for a delayed rise and a slower population decay. The energy relaxation is more pronounced than at low coverages, so that, below the peak maximum, the relaxation of the states directly populated in the optical transition feeds the lower lying states. The energy relaxation probably results from the prompt nuclear motion induced by the charge-transfer excitation between two states with displaced potential minima. Most significantly, the long time scale population relaxation at energies 0.1−0.2 eV below the vertical excitation energy in Figure 19 is considerably slower for the deuterated molecule, which provides clear evidence for a significant deuterium isotope effect.[31]

The tendency for increased stabilization of the wet electron resonance continues when coverages are increased to 2 ML (Figure 19c), even though the resonance intensity is attenuated in the 2PP spectra. Lifetime of the long-lived component extends beyond 100 fs. The longer lifetimes make it possible to identify a slower energy relaxation process, which occurs at a rate of <0.1 eV/100 fs. At even higher coverages, a fraction of the excited-state population that survives the initial (<50 fs) energy and population relaxation processes is stabilized in a state ∼2 eV above E_F on the picosecond time scale.[239]

The observed dynamics for CH_3OH and CH_3OD overlayers can be summarized in terms of the following key processes. At early times, the excited-state evolves through rapid population and energy relaxation processes on 20−30 fs time scales. The time scales for both processes are comparable, and their contributions are energy-dependent, which makes it difficult to specify separate rates for each process. After the initial energy relaxation of ∼0.2 eV, the excited state for >1 ML methanol coverage becomes more stable with respect to the population decay. The quasi-stable state that forms after ∼50 fs undergoes a slower (<0.1 eV/100 fs) energy relaxation process and a population decay that exhibits a pronounced D isotope effect.

The individual population and energy relaxation processes that contribute to the overall dynamics of the wet electron states can be summarized in the schematic diagram in Figure 20. The primary excitation process involves photoinduced

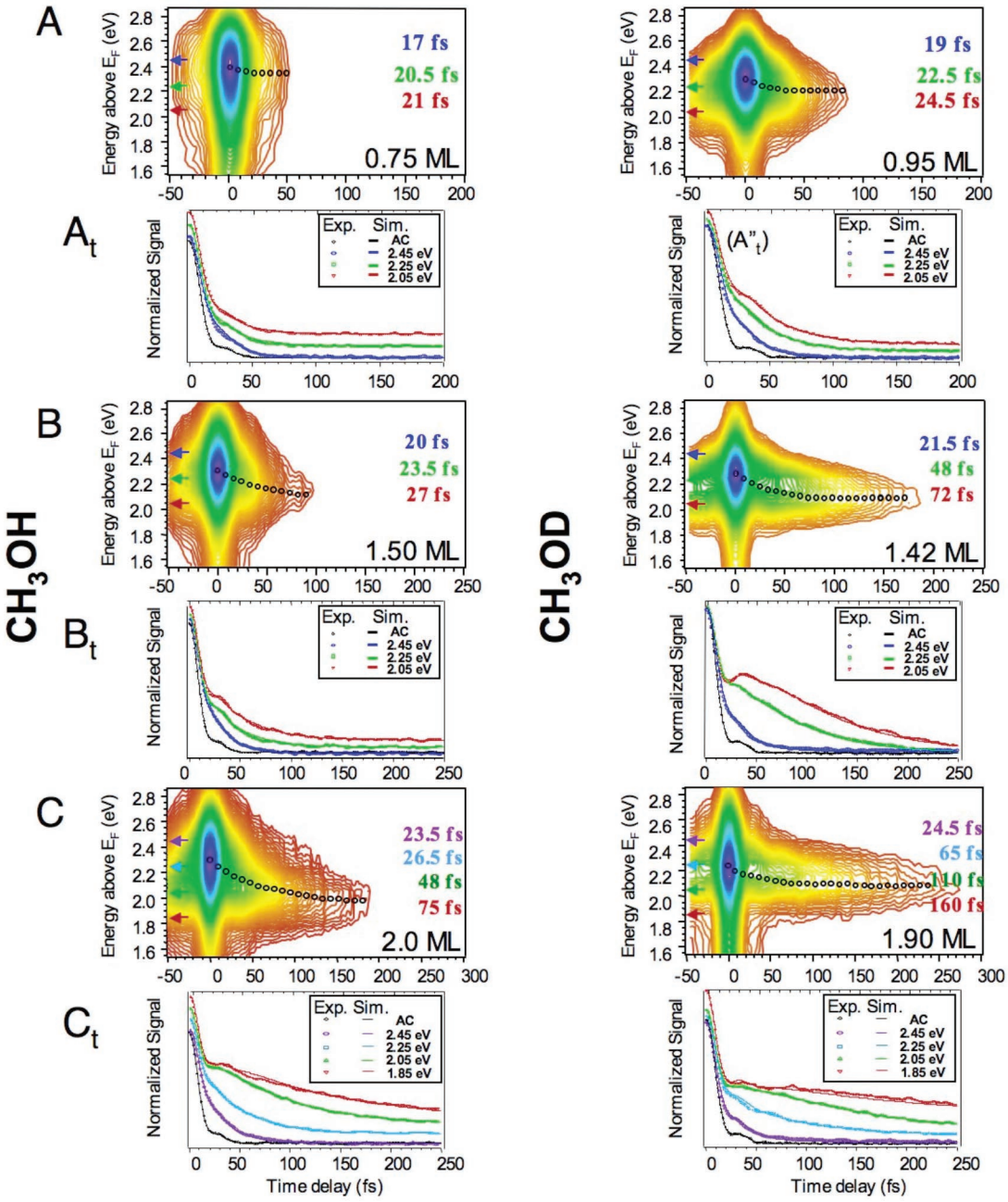

Figure 19. Three-dimensional plots showing the wet electron state dynamics for CH_3OH (left) and CH_3OD (right) overlayers on TiO_2 in (a) <1 ML, (b) ~1.5 ML, and (c) ~2 ML regimes. The 3D plots are constructed from pump−probe measurements at different energies such as shown for several characteristic energies below each 3D plot. The circles indicate the energy stabilization of the wet electron resonance at increasing delays.[31]

charge transfer from the Ti 3d defect band where the charge is distributed over several Ti_{5c}^{4+} sites[232] to the CH_3OH overlayer. The charge-transfer excitation occurs nonadiabatically, creating an excited-state wave packet N_1 with ground-state geometry on the excited-state surface that is displaced from its equilibrium geometry along several coordinates. These coordinates are related to the creation of the hole in the TiO_2 substrate and injection of an electron into the molecular overlayer. The creation of a hole drives the relaxation of the TiO_2 lattice, involving primarily the Ti−O bond stretching vibrations.[232] Likewise, the injection of electrons into the molecular overlayer elicits the motion of the electropositive H atoms. Both motions lead to the dielectric screening of the photogenerated charge distribution and therefore can be responsible for the fast energy relaxation. However, because the D isotope substitution effect is not strongly evident in the fast dynamics, it appears that the heavy atom motions determine the rate of the primary energy relaxation process, as is often observed in molecular proton-transfer processes such as photoinduced tautomerization.[244] Moreover, the time and energy scales for the primary energy relaxation process are consistent with the polaron formation in TiO_2.[31,245]

The excited-state energy and population decay dynamics can be recast in terms of displaced free-energy curves for the ground-state-donor and excited-state-acceptor potential surfaces, which are coupled through a generalized solvent coordinate, as is often done in the Marcus−Jortner theory for electron transfer.[36,246−248] In Figure 21, we plot such surfaces for free-energy states that represent the ground (1a) and excited (2b) states for photoinduced charge transfer, where both the electron and proton (hydrogen) are displaced

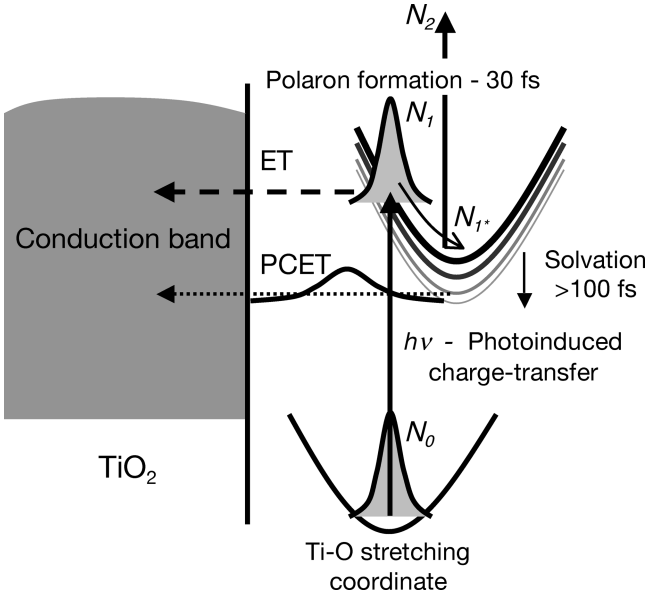

Figure 20. Schematic energy diagram for the 2PP excitation that measures the population and energy relaxation processes for electrons injected into CH_3OH and CH_3OD overlayers on TiO_2. The optical charge-transfer excitation occurs between states that are displaced along heavy-atom (Ti−O) coordinates. Initial energy relaxation from the photoexcited state N_1 to a quasi-stationary state N_{1*} by polaron formation is followed by slower solvation. The population relaxation is transformed from the nonadiabatic to proton-coupled RCT regime through the polaron formation.[31] N_0 and N_2 refer to the initial and final states in the 2PP process.

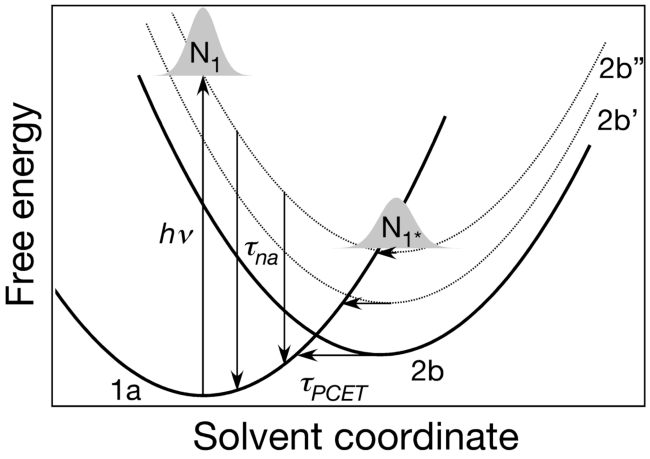

Figure 21. Free-energy surfaces for the nonadiabatic and proton-coupled electron transfer following the photoinduced charge-transfer excitation of an electron into a CH_3OH overlayer on TiO_2, as explained in the text.[31]

from their ground-state position. To describe the displacement of both electrons and protons, we generally need four separate potentials to describe the transfer of single particles, and transfer of both particles, which are coupled by two solvent coordinates.[247,248] However, because we cannot specify with certainty how the transfer proceeds, we show only the initial and final states. The photoinduced charge transfer occurs vertically, creating an excited-state wave packet N_1, which is displaced along the solvent coordinate from the equilibrium geometry of the excited state. In addition, the excited state can be displaced along other internal coordinates involving the displacement of H atoms from their excited-state equilibrium positions, which we represent with as manifold of excited-state free-energy surfaces (2b, 2b′, and 2b″). The initially created wave packet evolves on this manifold along the solvent coordinate, leading to the dielectric screening of the photoinduced charge distribution by the heavy atom motion to form a quasi-stationary N_{1*} state.

Simultaneously with the screening of the charge distribution, the excited state can decay through the nonadiabatic RCT (vertical downward transitions in Figure 21) into the CB of TiO_2. After the vertical excitation and before the inertial response of the interface is complete, the nonadiabatic decay is exothermic and the transition moment is favorable.[31]

As a result of these energy and population relaxation processes, the excited state is brought to a quasi-stable state from which further relaxation is substantially suppressed. For large displacements from the ground-state geometry, according to Figure 21, the nonadiabatic decay can become endothermic, leading to the stabilization of the charge-transferred state. However, adiabatic proton-coupled electron transfer (PCET; horizontal arrows in Figure 21) is favorable near the crossings between the 1a and 2b manifolds. The continuing energy relaxation of the quasi-stable state observed in experiments can be attributed to electron solvation by the molecular overlayer. The precise rate of energy relaxation is difficult to quantify because the measurements are limited to delays of 250 fs. However, the lack of pronounced energy relaxation is consistent with the solvation through the translation and diffusion of methanol.[120]

5.3.3. Proton-Coupled Electron Transfer

Perhaps the most interesting part of the solvation dynamics in the methanol overlayer is the deuterium isotope effect on the population dynamics, which is responsible for the significantly slower wet electron population decay for CH_3OD in Figure 19.[31] Simulation of the energy and population dynamics for electrons injected into methanol overlayers at different energies that span the resonance with an exponential decay for the primary photoexcited state N_1 and a fast exponential rise and a slower decay of the quasistationary state N_{1*} for CH_3OH and CH_3OD overlayers under similar coverage conditions quantify the magnitude of the D isotope effect. The plot of CH_3OD decay time constants versus those for CH_3OH under similar conditions in Figure 22 indicates essentially no isotope effect on the primary decay/rise and a ratio of D/H time constants of 2.2 for the decay of the quasistationary state. Because the decay of the quasistationary state is mainly due to the population decay, the observed D isotope effect suggests that the RCT process from the N_{1*} state is coupled with the proton or hydrogen motion in the methanol overlayer. Such dynamics involving the coupling of electron and proton motion have been extensively investigated in solution phase and are thought to play an important role in many biological processes such as photosynthesis and respiration.[249] Strong deuterium isotope effects are known in the electron-stimulated desorption of H^+/D^+ from metal surfaces, where the survival probability of ions exponentially depends upon the escape velocity of ions.[250] However, the CH_3OH/TiO_2 system presents the first example of PCET in a heterogeneous photoinduced charge-transfer process, where proton motion controls the rate of RCT.[247,248,251,252] Other possible population decay channels such as $e-e$ scattering are not coupled with the nuclear motion.[253]

The magnitude of the isotope effect provides further information on kinetic processes that may be responsible for the correlated dynamics of electrons and protons. If the

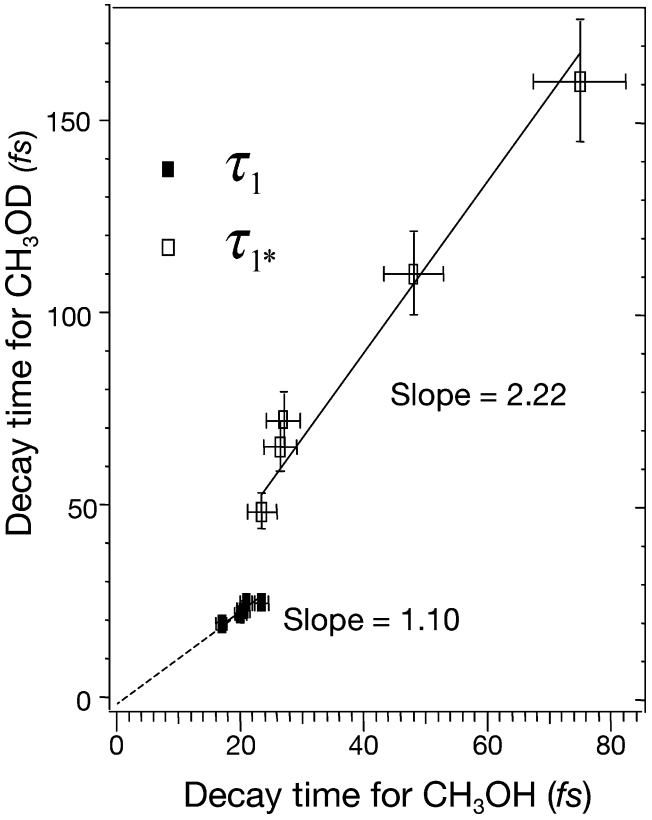

Figure 22. Decay times of CH_3OD for the primary, vertically excited state (■) and secondary, quasistationary state (□) versus the decay times under comparable coverage and energy conditions for CH_3OH. The deviation of the slopes from 1 quantifies the observed isotope effects.[31]

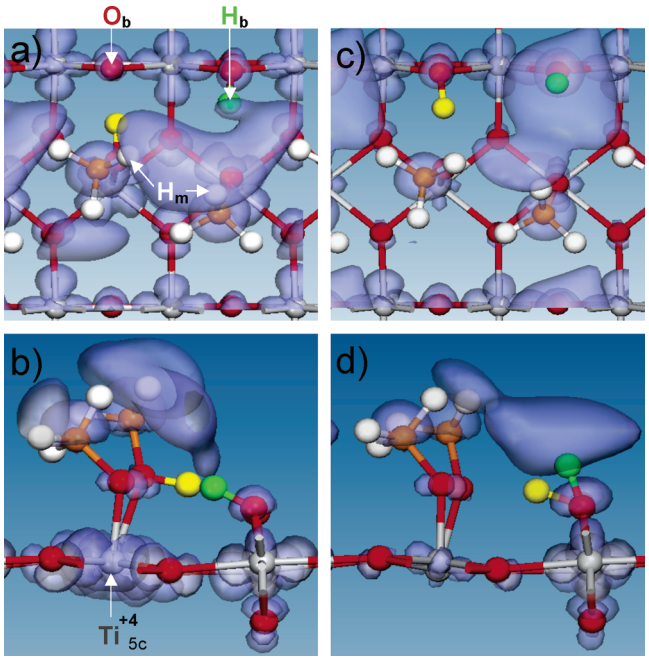

Figure 23. Results of the Δ-SCF calculation for 50% dissociated 1 ML coverage of CH_3OH on TiO_2.[31] Left panels show the top and side views for the ground-state geometry, and the right panels show the optimized geometry after adding an electron to the unoccupied wet electron orbital. The wet electron orbital is indicated as a translucent cloud. The structure optimization leads to large displacements of H atoms on the bridging −OH (green) and methanol OH (yellow). The H atom displacements are correlated with the descent of the excess electron toward the surface. Methyl H atoms are indicated by white; C atoms are orange; O atoms are red; and Ti atoms are gray.

isotope effect is only given by the relative velocity of protons and deuterons, the ratio of the observed decay time constants can be given at most by $\sqrt{m_D/m_H}$, where m_H and m_D represent the reduced masses for the relevant nuclear motion in deuterated and protonated overlayers that is correlated with the RCT. The maximum value for the D isotope effect related to the relative motion of D to H atoms is $\sqrt{2}$.[87,92,93] Because the observed ratio is substantially larger than this limit, PECT cannot be related simply to the free motion of single protons and deuterons.

In the literature on PECT, many other kinetic mechanisms have been proposed to explain isotope effects that are larger than the $\sqrt{2}$ limit for the free motion of H/D.[251,252] In the case of RCT from CH_3OH overlayers, these could include differences in the zero-point energies for the H/D motions, tunneling through a barrier, the correlated motion of several H/D atoms, etc. The exact origin of the isotope effect on RCT in the CH_3OH/TiO_2 system is yet to be determined.[31]

However, the role of H/D motion in PECT for the CH_3OH/TiO_2 system can be gleaned from Δ-SCF calculations on the optimized excited-state structure for 1 ML CH_3OH coverage on a single layer TiO_2, where in the ground state, 50% of the molecules are dissociated.[31] In this calculation, first the ground-state structure of a 50% dissociated CH_3OH overlayer was calculated by DFT. Then, the optimized structure of the CH_3OH overlayer on a single TiO_2 layer was extracted from the DFT calculation (parts a and b of Figure 23). The unoccupied wet electron state was identified in the same manner as for the H_2O/TiO_2 system,[186] and an electron was added to the unoccupied orbital. As discussed in ref 31, this anionic state is not the true charge-transfer excitation excited state. The calculation assumes that the hole decay is much faster and uncorrelated with the electron decay. After the extra electron was added, the excited-state structure of the CH_3OH overlayer was reoptimized, while keeping the TiO_2 surface layer fixed. The success of the calculation hinges on the weak hybridization of the electron in the molecular overlayer with the large density of isoenergetic CB states of TiO_2 to keep the electron from decaying from the overlayer into the substrate.

The starting and end points of the Δ-SCF calculation in parts a and b of Figure 23 reveal how the electron interacts with the CH_3OH molecules at these stages of the structure optimization. Initially, for the ground-state molecular structure, the unoccupied electron orbital is mainly associated with the H_m atoms of the methyl groups on the chemisorbed methanol and the methoxy species. The participation of H_m atoms in the solvation of electrons, when the more favorable OH species are engaged in strong HBs, has been proposed in theoretical calculations on methanol anion clusters and is evident in the resonance Raman spectra of solvated electrons in alcohols.[106,107]

The structural changes caused by the introduction of an excess electron into the CH_3OH overlayer can be tracked for each optimization cycle of the Δ-SCF calculation. The relative motions and time ordering for specific atoms in the optimization provide insight into the driving forces for the structural change. Parts c and d of Figure 23 reveal that the main response of the CH_3OH overlayer involves the breaking of existing HBs to stabilize the energy of the excess charge. The primary H atom motion (green) involves the rotation of the bridging −OH species from the ground-state orientation,

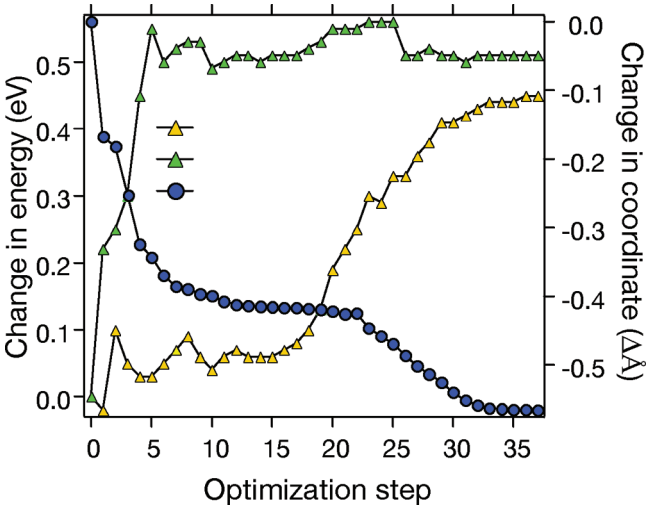

Figure 24. Change in the total energy during the Δ-SCF optimization (blue circles; left axis) and the displacement (right axis) of the green and yellow H atoms (indicated in Figure 23) as a function of the optimization step. The primary excited-state stabilization is achieved by the motion of the bridging H atom (green), followed by the deprotonation of methanol (yellow).

where it forms a HB with the proximate $-OCH_3$, to a nearly surface normal position. This motion leads to ~70% of the total excited-state stabilization of ~0.6 eV (Figure 24). Further stabilization is achieved by the deprotonation of CH_3OH to form a bridging $-OH$ (yellow).[31]

In the final structure of the Δ-SCF calculation, 100% of CH_3OH is dissociated; however, the two molecules in the unit cell are not equivalent. Apparently, the primary motion of the bridging $-OH$ is strongly correlated with the excess charge: breaking of the HB with the $-OCH_3$ species provides a favorable site for the electron to localize closer to the surface. The secondary proton transfer occurs in response to the new charge distribution; however, with the electron localized above the primary $-OH$, the dissociation of the HB after the secondary proton transfer does not occur.

The net result of the correlated electron−proton motion is that the electron descends from the H_m atoms, where it is shielded from the CB of TiO_2 to the surface $-OH$ species. Because the RCT from similar bridging $-OH$ sites on $H/H_2O/TiO_2$ surfaces occurs in 15 fs, it can be argued that the final state of the Δ-SCF calculation is less stable with respect to RCT. Thus, the correlated motion of electrons and protons upon the injection of charge into the protic solvent overlayer can promote D-isotope-dependent RCT.

The TR-2PP studies of reduced H_2O- and CH_3OH-covered TiO_2 surfaces provide a glimpse of the molecular response to the injection of charge that is relevant to photocatalytic processes on metal oxide surfaces. The nonadiabatic injection of charge (electron or hole) is likely to have a profound impact on the existing HB network at metal oxide−protic solvent interfaces. The correlated motion of protons in response of the excess charge that has been vividly uncovered through TR-2PP measurements and DFT theory is likely to be an integral aspect of photocatalytic reactions on protic-solvent-covered metal oxide surfaces. For instance, the correlated motion of protons and electrons is necessary for the photoelectrochemical splitting of H_2O into H_2 and O_2, which occurs without an external bias for band-gap excitation of anatase single crystals.[254] Also, methanol plays an important role in photocatalysis as a sacrificial agent.[255] TR-2PP studies along with DFT calculations on model systems such as H_2O and CH_3OH on TiO_2(110) provide for the first time a molecular-level view of the photophysical and photochemical processes that drive photocatalysis. Moreover, the wet electron states that have been identified on H_2O and CH_3OH overlayers should be ubiquitous on protic-solvent-covered metal oxide surfaces. The studies on TiO_2 demonstrate that for CH_3OH multilayer coverage it is possible to stabilize electrons 2 eV above the Fermi level on picosecond time scales. Such electrons should be powerful reducing agents that can drive a variety of chemical reactions through the dissociative electron attachment.[129,219,256−258] Such presolvated electrons in water and ice films may play an important role in the chemistry of Freons on the stratospheric cloud ice surfaces and therefore contribute to the ozone destruction cycle.[259] We note, however, that both H_2O and CH_3OH overlayer films on TiO_2 are stable with respect to the photochemical decomposition under the conditions for measuring 2PP spectra.

Moreover, TR-2PP measurements reveal the role of the H atom acceptor in interfacial charge-transfer processes. The RCT rates from tightly bound H atoms on the bridging rows are extremely fast, but they are surprisingly slow in light of the reported <10 fs charge injection from photoexcited dye molecules into the CB of TiO_2 nanocolloids and single-crystal surfaces.[260−263] Considering the likely termination of TiO_2 with surface $-OH$ species upon chemisorption of OH-containing molecules or in protic solvents, it is possible that the wet electron states mediate interfacial charge transfer from dye molecules. The role of surface termination is likely to be reveled through TR-2PP measurements on well-defined TiO_2 surfaces that have been prepared through rigorous surface science protocols.[229,264] The future role of TR-2PP measurements in elucidating the charge transport in photocatalytic and photovoltaic processes on metal oxide electrodes is bright.

6. Conclusions and Future Perspectives

The interaction of electrons and protons in protic solvents is pervasive in chemistry and physics. Detailed information on solvated electrons has been obtained from solution-phase, cluster, and surface studies. The cluster studies bring out the dichotomy of surface versus bulk solvation that is likely to have broad significance in the context of biology, electrochemistry, catalysis, environmental chemistry, etc. In particular, the 2D solvated electrons at solvent surfaces may be particularly reactive metastable reagents that can participate in a variety of interfacial reactions.

The marriage of surface science techniques with ultrafast spectroscopy provides a powerful means for preparing well-defined molecular-film samples, in which it is possible to investigate with a great degree of control the surface and bulk solvation. With extreme time resolution, it is possible to resolve the fundamental molecular response to the presence of excess charge and relate the observed phenomena to theoretical models of the molecular and electronic structure of ideal surfaces. Because metal oxide surfaces are prevalent in environmentally and technologically important settings, the discovery of wet electrons in hydrous overlayers is likely to be crucial to elucidating many important interfacial phenomena that are driven by light or other forms of electronic excitation. TR-2PP spectroscopy of well-defined metal and metal oxide surfaces offers a powerful means for investigation of the electronic structure, charge-transfer dynamics, and presolvated electron-induced chemistry of

relevance to topical issues such as photocatalytic and photovoltaic energy conversion.

7. Acknowledgment

The authors gratefully acknowledge the significant contributions of Profs. K. D. Jordan and J. Yang to the theoretical investigations of wet electron states on metal oxides. H. Petek thanks Prof. M. Wolf and Dr. U. Bovensiepen for their critical comments on the discussion of the electron solvation in H_2O overlayers on metals and Prof. John T. Yates, Jr. for his patience and encouragement. This work was supported by the DoD MURI program under Grant DAAD19-01-1-0619, New Energy Development Organization of Japan "Molecular wire" project) and PRF Grant number 44158-AC5. Some of the calculations described in this review were performed in the Environmental Molecular Sciences Laboratory, a national scientific user facility sponsored by the Department of Energy's Office of Biological and Environmental Research and located at Pacific Northwest National Laboratory.

8. References

(1) Weyl, W. *Ann. Phys. (Leipzig)* **1864**, *121*, 601.
(2) Kraus, C. *J. Am. Chem. Soc.* **1908**, *30*, 1323.
(3) Hart, E. J.; Anbar, M. *The Hydrated Electron*; Wiley-Interscience: New York, 1970.
(4) Garrett, B. C.; Dixon, D. A.; Camaioni, D. M.; Chipman, D. M.; Johnson, M. A.; Jonah, C. D.; Kimmel, G. A.; Miller, J. H.; Rescigno, T. N.; Rossky, P. J.; Xantheas, S. S.; Colson, S. D.; Laufer, A. H.; Ray, D.; Barbara, P. F.; Bartels, D. M.; Becker, K. H.; Bowen, H.; Bradforth, S. E.; Carmichael, I.; Coe, J. V.; Corrales, L. R.; Cowin, J. P.; Dupuis, M.; Eisenthal, K. B.; Franz, J. A.; Gutowski, M. S.; Jordan, K. D.; Kay, B. D.; LaVerne, J. A.; Lymar, S. V.; Madey, T. E.; McCurdy, C. W.; Meisel, D.; Mukamel, S.; Nilsson, A. R.; Orlando, T. M.; Petrik, N. G.; Pimblott, S. M.; Rustad, J. R.; Schenter, G. K.; Singer, S. J.; Tokmakoff, A.; Wang, L. S.; Wittig, C.; Zwier, T. S. *Chem. Rev.* **2005**, *105*, 355.
(5) Pshenichnikov, M. S.; Baltuska, A.; Wiersma, D. A. *Topics in Applied Physics*; Kärtner, F. X., Eds.; Springer-Verlag: Berlin, Germany, 2004; Vol. 95.
(6) Hart, E. J.; Boag, J. W. *J. Am. Chem. Soc.* **1962**, *84*, 4090.
(7) Boag, J. W.; Hart, E. J. *Nature* **1963**, *197*, 45.
(8) Marcus, R. A. *J. Chem. Phys.* **1965**, *43*, 679.
(9) Kasinski, J. J.; Gomez-Jahn, L. A.; Faran, K. J.; Gracewski, S. M.; Miller, R. J. D. *J. Chem. Phys.* **1989**, *90*, 1253.
(10) Lewis, N. S. *Annu. Rev. Phys. Chem.* **1991**, *42*, 543.
(11) Benjamin, I. *Chem. Rev.* **1996**, *96*, 1449.
(12) Fujishima, A.; Hashimoto, K.; Watanabe, H., *Photocatalysis: Fundamentals and Applications*; BKC, Inc.: Tokyo, Japan, 1997.
(13) Ehrenfreund, P.; Irvine, W.; Becker, L.; Blank, J.; Brucato, J. R.; Colangeli, L.; Derenne, S.; Despois, D.; Dutrey, A.; Fraaije, H.; Lazcano, A.; Owen, T.; Robert, F.; Issi-Team *Rep. Prog. Phys.* **2002**, 1427.
(14) Dominguez-Ariza, D.; Hartnig, C.; Sousa, C.; Illas F., *J. Chem. Phys.* **2004**, *121*, 1066.
(15) Anderson, N. A.; Lian, T. *Annu. Rev. Phys. Chem.* **2005**, *56*, 491.
(16) Vassilev, P.; van Santen, R. A.; Koper, M. T. M. *J. Chem. Phys.* **2005**, *122*, 054701.
(17) Taylor, C. D.; Wasileski, S. A.; Filhol, J.-S.; Neurock, M. *Phys. Rev. B* **2006**, *73*, 165402.
(18) Taylor, C. D.; Neurock, M. *Curr. Opin. Solid State Mater. Sci.* **2005**, *9*, 49.
(19) Kolasinski, K. W. *Curr. Opin. Solid State Mater. Sci.* **2005**, *9*, 8.
(20) Jungwirth, P.; Finlayson-Pitts, B. J.; Tobias, D. J. *Chem. Rev.* **2006**, *106*, 1137.
(21) Shen, Y. R.; Ostroverkhov, V. *Chem. Rev.* **2006**, *106*, 1140.
(22) Winter, B.; Faubel, M. *Chem. Rev.* **2006**, *106*, 1176.
(23) Mundy, C. J.; Kuo, I. F. W. *Chem. Rev.* **2006**, *106*, 1282.
(24) Benjamin, I. *Chem. Rev.* **2006**, *106*, 1212.
(25) Ewing, G. E. *Chem. Rev.* **2006**, *106*, 1511.
(26) Verdaguer, A.; Sacha, G. M.; Bluhm, H.; Salmeron, M. *Chem. Rev.* **2006**, *106*, 1478.
(27) Makov, G.; Nitzan, A. *J. Phys. Chem.* **1994**, *98*, 3459.
(28) Park, C.; Fenter, P. A.; Nagy, K. L.; Sturchio, N. C. *Phys. Rev. Lett.* **2006**, *97*, 016101.
(29) Ge, N.-H.; Wong, C. M.; Lingle, R. L., Jr.; McNeill, J. D.; Gaffney, K. J.; Harris, C. B. *Science* **1998**, *279*, 202.
(30) Gahl, C.; Bovensiepen, U.; Frischkorn, C.; Wolf, M. *Phys. Rev. Lett.* **2002**, *89*, 107402.
(31) Li, B.; Zhao, J.; Onda, K.; Jordan, K. D.; Yang, J.; Petek, H. *Science* **2006**, *311*, 1436.
(32) Haight, R. *Surf. Sci. Rep.* **1995**, *21*, 275.
(33) Petek, H.; Ogawa, S. *Prog. Surf. Sci.* **1997**, *56*, 239.
(34) Weinelt, M. *J. Phys.: Condens. Matter* **2002**, *14*, R1099.
(35) Zhu, X.-Y. *Annu. Rev. Phys. Chem.* **2002**, *53*, 221.
(36) Zhu, X. Y. *Surf. Sci. Rep.* **2004**, *56*, 1.
(37) Harris, C. B.; Ge, N.-H.; Lingle, R. L.; McNeill, J. D. *Annu. Rev. Phys. Chem.* **1997**, *48*, 711.
(38) Höfer, U. *Science* **1998**, *279*, 190.
(39) Machado, M.; Chulkov, E. V.; Silkin, V. M.; Höfer, U.; Echenique, P. M. *Prog. Surf. Sci.* **2003**, *74*, 219.
(40) Güdde, J.; Höfer, U. *Prog. Surf. Sci.* **2005**, *80*, 49.
(41) Bovensiepen, U. *Prog. Surf. Sci.* **2005**, *78*, 87.
(42) Szymanski, P.; Garrett-Roe, S.; Harris, C. B. *Prog. Surf. Sci.* **2005**, *78*, 1.
(43) Bovensiepen, U. Habilitation Thesis, Free University Berlin, Berlin, Germany, 2005.
(44) Merry, W. R.; Jordan, R. E.; Padowitz, D. F.; Harris, C. B. *Surf. Sci.* **1993**, *295*, 393.
(45) McNeill, J. D.; Lingle, R. L.; Jordan, R. E.; Padowitz, D. F.; Harris, C. B. *J. Chem. Phys.* **1996**, *105*, 3883.
(46) McNeill, J. D.; Lingle, R. L.; Ge, N.-H.; Wong, C. M.; Jordan, R. E.; Harris, C. B. *Phys. Rev. Lett.* **1997**, *79*, 4645.
(47) Wolf, M.; Knoesel, E.; Hertel, T. *Phys. Rev. B* **1996**, *54*, R5295.
(48) Berthold, W.; Feulner, P.; Höfer, U. *Chem. Phys. Lett.* **2002**, *358*, 502.
(49) Rohleder, M.; Berthold, W.; Gudde, J.; Höfer, U. *Phys. Rev. Lett.* **2005**, *94*, 017401.
(50) Lingle, J. R. L.; Padowitz, D. F.; Jordan, R. E.; McNeill, J. D.; Harris, C. B. *Phys. Rev. Lett.* **1994**, *72*, 2243.
(51) Hotzl, A.; Ishioka, K.; Knoesel, E.; Wolf, M.; Ertl, G. *Chem. Phys. Lett.* **1998**, *291*, 573.
(52) Wang, H.; Dutton, G.; Zhu, X.-Y. *J. Phys. Chem. B* **2000**, *104*, 10332.
(53) Miller, A. D.; Gaffney, K. J.; Liu, S. H.; Szymanski, P.; Garrett-Roe, S.; Wong, C. M.; Harris, C. B. *J. Phys. Chem. A* **2002**, *106*, 7636.
(54) Dutton, G.; Zhu, X.-Y. *J. Phys. Chem. B* **2002**, *106*, 5975.
(55) Zhong, Q.; Gahl, C.; Wolf, M. *Surf. Sci.* **2002**, *496*, 21.
(56) Miller, A. D.; Bezel, I.; Gaffney, K. J.; Garrett-Roe, S.; Liu, S. H.; Szymanski, P.; Harris, C. B. *Science* **2002**, *297*, 5584.
(57) Liu, S. H.; Miller, A. D.; Gaffney, K. J.; Szymanski, P.; Garrett-Roe, S.; Bezel, I.; Harris, C. B. *J. Phys. Chem. B* **2002**, *106*, 12908.
(58) Gahl, C.; Bovensiepen, U.; Frischkorn, C.; Morgenstern, K.; Rieder, K.-H.; Wolf, M. *Surf. Sci.* **2003**, *532*−*535*, 108.
(59) Bovensiepen, U.; Gahl, C.; Wolf, M. *J. Phys. Chem. B* **2003**, *107*, 8706.
(60) Bovensiepen, U.; Gahl, C.; Stähler, J.; Wolf, M. *Surf. Sci.* **2005**, *584*, 90.
(61) Onda, K.; Li, B.; Zhao, J.; Petek, H. *Surf. Sci.* **2005**, *593*, 32.
(62) Onda, K.; Li, B.; Zhao, J.; Jordan, K. D.; Yang, J.; Petek, H. *Science* **2005**, *308*, 1154.
(63) Stähler, J.; Gahl, C.; Bovensiepen, U.; Wolf, M. *J. Phys. Chem. B* **2006**, *110*, 9637.
(64) Fox, M. A.; Dulay, M. T. *Chem. Rev.* **1993**, *93*, 341.
(65) Hoffmann, M. R.; Martin, S. T.; Choi, W.; Bahnemann, D. W. *Chem. Rev.* **1995**, *95*, 69.
(66) Linsebigler, A. L.; Lu, G.; Yates, J. T., Jr. *Chem. Rev.* **1995**, *95*, 735.
(67) Thompson, T. L.; Yates, J. T., Jr. *Top. Catal.* **2005**, *35*, 197.
(68) Turi, L.; Sheu, W.-S.; Rossky, P. J. *Science* **2005**, *309*, 914.
(69) Verlet, J. R. R.; Bragg, A. E.; Kammrath, A.; Cheshnovsky, O.; Neumark, D. M. *Science* **2005**, *307*, 93.
(70) Silvestrelli, P. L.; Parrinello, M. *Phys. Rev. Lett.* **1999**, *82*, 3308.
(71) Badyal, Y. S.; Saboungi, M. L.; Price, D. L.; Shastri, S. D.; Haeffner, D. R.; Soper, A. K. *J. Chem. Phys.* **2000**, *112*, 9206.
(72) Matsumoto, M.; Saito, S.; Ohmine, I. *Nature* **2002**, *416*, 409.
(73) Head-Gordon, T.; Hura, G. *Chem. Rev.* **2002**, *102*, 2651.
(74) Chen, B.; Ivanov, I.; Klein, M. L.; Parrinello, M. *Phys. Rev. Lett.* **2003**, *91*, 215503.
(75) Wernet, P.; Nordlund, D.; Bergmann, U.; Cavalleri, M.; Odelius, M.; Ogasawara, H.; Naslund, L. A.; Hirsch, T. K.; Ojamae, L.; Glatzel, P.; Pettersson, L. G. M.; Nilsson, A. *Science* **2004**, *304*, 995.
(76) Smith, J. D.; Cappa, C. D.; Wilson, K. R.; Messer, B. M.; Cohen, R. C.; Saykally, R. J. *Science* **2004**, *306*, 851.
(77) Nilsson, A.; Wernet, P.; Nordlund, D.; Bergmann, U.; Cavalleri, M.; Odelius, M.; Ogasawara, H.; Naslund, L. A.; Hirsch, T. K.; Ojamae, L.; Glatzel, P.; Pettersson, L. G. M. *Science* **2005**, *308*, 793a.

(78) Smith, J. D.; Cappa, C. D.; Messer, B. M.; Cohen, R. C.; Saykally, R. J. *Science* **2005**, *308*, 793b.
(79) Head-Gordon, T.; Johnson, M. E. *Proc. Natl. Acad. Sci. U.S.A.* **2006**, *103*, 7973.
(80) Tsurusawa, T.; Iwata, S. *Chem. Phys. Lett.* **1999**, *315*, 433.
(81) Zhan, C. G.; Dixon, D. A. *J. Phys. Chem. B* **2003**, *107*, 4403.
(82) Jortner, J.; Noyes, R. M. *J. Phys. Chem.* **1966**, *70*, 770.
(83) Coe, J. V. *Int. Rev. Phys. Chem.* **2001**, *20*, 33.
(84) Migus, A.; Gauduel, Y.; Martin, J. L.; Antonetti, A. *Phys. Rev. Lett.* **1987**, *58*, 1559.
(85) Alfano, J. C.; Walhout, P. K.; Kimura, Y.; Barbara, P. F. *J. Chem. Phys.* **1993**, *98*, 5996.
(86) Silva, C.; Walhout, P. K.; Yokoyama, K.; Barbara, P. F. *Phys. Rev. Lett.* **1998**, *80*, 1086.
(87) Yokoyama, K.; Silva, C.; Son, D. H.; Walhout, P. K.; Barbara, P. F. *J. Phys. Chem. A* **1998**, *102*, 6957.
(88) Emde, M. F.; Baltuska, A.; Kummrow, A.; Pshenichnikov, M. S.; Wiersma, D. A. *Phys. Rev. Lett.* **1998**, *80*, 4645.
(89) Baltuska, A.; Emde, M. F.; Pshenichnikov, M. S.; Wiersma, D. A. *J. Phys. Chem. A* **1999**, *103*, 10065.
(90) Assel, M.; Laenen, R.; Laubereau, A. *J. Chem. Phys.* **1999**, *111*, 6869.
(91) Laenen, R.; Roth, T.; Laubereau, A. *Phys. Rev. Lett.* **2000**, *85*, 50.
(92) Pshenichnikov, M. S.; Baltuska, A.; Wiersma, D. A. *Chem. Phys. Lett.* **2004**, *389*, 171.
(93) Barnett, R. B.; Landman, U.; Nitzan, A. *J. Chem. Phys.* **1989**, *90*, 4413.
(94) Kevan, L. *Acc. Chem. Res.* **1981**, *14*, 138.
(95) Schnitker, J.; Rossky, P. J. *J. Chem. Phys.* **1987**, *86*, 3471.
(96) Schnitker, J.; Motakabbir, K.; Rossky, P. J.; Friesner, R. A. *Phys. Rev. Lett.* **1988**, *60*, 456.
(97) Ludwig, V.; Coutinho, K.; Canuto, S. *Phys. Rev. B* **2004**, *70*, 214110.
(98) Lindner, J.; Unterreiner, A.-N.; Vöhringer, P. *ChemPhysChem* **2006**, *7*, 363.
(99) Shkrob, I. A. *J. Phys. Chem. A* **2006**, *110*, 3967.
(100) Kim, K. S.; Park, I.; Lee, S.; Cho, K.; Lee, J.; Kim, J.; Joannopoulos, J. D. *Phys. Rev. Lett.* **1996**, *76*, 956.
(101) Fortes, A. D.; Brodholt, J. P.; Wood, I. G.; Vocadlo, L. *J. Chem. Phys.* **2003**, *118*, 5987.
(102) Sprik, M.; Impey, R. W.; Klein, M. L. *J. Chem. Phys.* **1985**, *83*, 5802.
(103) Barnett, R. N.; Landman, U.; Nitzan, A. *J. Chem. Phys.* **1989**, *91*, 5567.
(104) Pagliai, M.; Cardini, G.; Righini, R.; Schettino, V. *J. Chem. Phys.* **2003**, *119*, 6655.
(105) Turi, L.; Mosyak, A.; Rossky, P. J. *J. Chem. Phys.* **1997**, *107*, 1970.
(106) Turi, L. *J. Chem. Phys.* **1999**, *110*, 10364.
(107) Tauber, M. J.; Stuart, C. M.; Mathies, R. A. *J. Am. Chem. Soc.* **2004**, *126*, 3414.
(108) Hameka, H. F.; Robinson, G. W.; Marsden, C. J. *J. Phys. Chem.* **1987**, *91*, 3150.
(109) Sobolewski, A. L.; Domcke, W. *J. Phys. Chem. A* **2002**, *106*, 4158.
(110) Mizuno, M.; Tahara, T. *J. Phys. Chem. A* **2003**, *107*, 2411.
(111) Tauber, M. J.; Mathies, R. A. *J. Am. Chem. Soc.* **2003**, *125*, 1394.
(112) Neumann, S.; Eisfeld, W.; Sobolewski, A.; Domcke, W. *Phys. Chem. Chem. Phys.* **2004**, *6*, 5297.
(113) Sprik, M.; Klein, M. L. *J. Chem. Phys.* **1988**, *89*, 1592.
(114) Staib, A.; Borgis, D. *J. Chem. Phys.* **1995**, *103*, 2642.
(115) Pepin, C.; Goulet, T.; Houde, D.; Jay-Gerin, J. P. *J. Phys. Chem. A* **1997**, *101*, 4351.
(116) Shi, X.; Long, F. H.; Lu, H.; Eisenthal, K. B. *J. Phys. Chem.* **1996**, *100*, 11903.
(117) Lian, R.; Crowell, R. A.; Shkrob, I. A. *J. Phys. Chem. A* **2005**, *109*, 1510.
(118) Walhout, P. K.; Alfano, J. C.; Kimura, Y.; Silva, C.; Reid, P. J.; Barbara, P. F. *Chem. Phys. Lett.* **1995**, *232*, 135.
(119) Silva, C.; Walhout, P. K.; Reid, P. J.; Barbara, P. F. *J. Phys. Chem. A* **1998**, *102*, 5701.
(120) Minary, P.; Turi, L.; Rossky, P. J. *J. Chem. Phys.* **1999**, *110*, 10953.
(121) Turi, L.; Minary, P.; Rossky, P. J. *Chem. Phys. Lett.* **2000**, *316*, 465.
(122) Scheidt, T.; Laenen, R. *Chem. Phys. Lett.* **2003**, *371*, 445.
(123) Turi, L.; Holpar, P.; Keszei, E. *J. Phys. Chem. A* **1997**, *101*, 5469.
(124) Mosyak, A. A.; Prezhdo, O. V.; Rossky, P. J. *J. Chem. Phys.* **1998**, *109*, 6390.
(125) Mosyak, A. A.; Prezhdo, O. V.; Rossky, P. J. *J. Mol. Struct.* **1999**, *485*−*486*, 545.
(126) Shi, X.; Long, F. H.; Lu, H.; Eisenthal, K. B. *J. Phys. Chem.* **1995**, *99*, 6917.
(127) Shirota, H.; Yoshihara, K.; Smith, N. A.; Lin, S.; Meech, S. R. *Chem. Phys. Lett.* **1997**, *281*, 27.
(128) Rodriguez, J.; Laria, D. *J. Phys. Chem. B* **2005**, *109*, 6473.
(129) Perry, C. C.; Faradzhev, N. S.; Fairbrother, D. H.; Madey, T. E. *Int. Rev. Phys. Chem.* **2004**, *23*, 289.
(130) Chander, M.; Li, Y. Z.; Patrin, J. C.; Weaver, J. H. *Phys. Rev. B* **1993**, *48*, 2493.
(131) Hong, Y. A.; Hahn, J. R.; Kang, H. *J. Chem. Phys.* **1998**, *108*, 4367.
(132) Hee Son, D.; Kambhampati, P.; Kee, T. W.; Barbara, P. F. *Chem. Phys. Lett.* **2001**, *342*, 571.
(133) Kambhampati, P.; Son, D. H.; Kee, T. W.; Barbara, P. F. *J. Phys. Chem. A* **2002**, *106*, 2374.
(134) Coe, J. V.; Lee, G. H.; Eaton, J. G.; Arnold, S. T.; Sarkas, H. W.; Bowen, K. H.; Ludewigt, C.; Haberland, H.; Worsnop, D. R. *J. Chem. Phys.* **1990**, *92*, 3980.
(135) Ayotte, P.; Johnson, M. A. *J. Chem. Phys.* **1997**, *106*, 811.
(136) Paik, D. H.; Lee, I.-R.; Yang, D.-S.; Baskin, J. S.; Zewail, A. H. *Science* **2004**, *306*, 672.
(137) Hammer, N. I.; Roscioli, J. R.; Bopp, J. C.; Headrick, J. M.; Johnson, M. A. *J. Chem. Phys.* **2005**, *123*.
(138) Tsurusawa, T.; Iwata, S. *Chem. Phys. Lett.* **1998**, *287*, 553.
(139) Jordan, K. D.; Wang, F. *Annu. Rev. Phys. Chem.* **2003**, *54*, 367.
(140) Lee, S.; Kim, J.; Lee, S. J.; Kim, K. S. *Phys. Rev. Lett.* **1997**, *79*, 2038.
(141) Byung, J. M.; Hyun, S. K.; Ho, S. K.; Chang, W. Y.; Kim, K. S. *Chem. Phys. Lett.* **1991**, *176*, 41.
(142) Novakovskaya, Y. V.; Stepanov, N. F. *Chem. Phys. Lett.* **2001**, *344*, 619.
(143) Lee, H. M.; Lee, S.; Kim, K. S. *J. Chem. Phys.* **2003**, *119*, 187.
(144) Hammer, N. I.; Shin, J.-W.; Headrick, J. M.; Diken, E. G.; Roscioli, J. R.; Weddle, G. H.; Johnson, M. A. *Science* **2004**, *306*, 675.
(145) Jordan, K. D. *Science* **2004**, *306*, 618.
(146) Barnett, R. N.; Landman, U.; Cleveland, C. L.; Jortner, J. *J. Chem. Phys.* **1988**, *88*, 4429.
(147) Verlet, J. R. R.; Bragg, A. E.; Kammrath, A.; Cheshnovsky, O.; Neumark, D. M. *Science* **2005**, *310*, 1769b.
(148) Turi, L.; Sheu, W.-S.; Rossky, P. J. *Science* **2005**, *310*, 1769c.
(149) Skorobogatiy, M.; Park, I. J.; Joannopoulos, J. D. *Comput. Mater. Sci.* **2005**, *32*, 96.
(150) Baletto, F.; Cavazzoni, C.; Scandolo, S. *Phys. Rev. Lett.* **2005**, *95*, 176801.
(151) Bragg, A. E.; Verlet, J. R. R.; Kammrath, A.; Cheshnovsky, O.; Neumark, D. M. *J. Am. Chem. Soc.* **2005**, *127*, 15283.
(152) Su, X.; Lianos, L.; Shen, Y. R.; Somorjai, G. A. *Phys. Rev. Lett.* **1998**, *80*, 1533.
(153) Richmond, G. L. *Chem. Rev.* **2002**, *102*, 2693.
(154) Wilson, K. R.; Schaller, R. D.; Co, D. T.; Saykally, R. J.; Rude, B. S.; Catalano, T.; Bozek, J. D. *J. Chem. Phys.* **2002**, *117*, 7738.
(155) Nordlund, D.; Ogasawara, H.; Wernet, P.; Nyberg, M.; Odelius, M.; Pettersson, L. G. M.; Nilsson, A. *Chem. Phys. Lett.* **2004**, *395*, 161.
(156) Kuo, I. F. W.; Mundy, C. J. *Science* **2004**, *303*, 658.
(157) Thiel, P. A.; Madey, T. E. *Surf. Sci. Rep.* **1987**, *7*, 211.
(158) Henderson, M. A. *Surf. Sci. Rep.* **2002**, *46*, 1.
(159) Fenter, P.; Sturchio, N. C. *Prog. Surf. Sci.* **2004**, *77*, 171.
(160) Thompson, T. L.; Yates, J. T., Jr. *Chem. Rev.* In press.
(161) Israelachvili, J.; Wennerstrom, H. *Nature* **1996**, *379*, 219.
(162) Pal, S. K.; Zewail, A. H. *Chem. Rev.* **2004**, *104*, 2099.
(163) Bagchi, B. *Chem. Rev.* **2005**, *105*, 3197.
(164) Stowell, M. H. B.; McPhillips, T. M.; Rees, D. C.; Soltis, S. M.; Abresch, E.; Feher, G. *Science* **1997**, *276*, 812.
(165) Kimmel, G. A.; Petrik, N. G.; Dohnalek, Z.; Kay, B. D. *Phys. Rev. Lett.* **2005**, *95*, 166102.
(166) Vonnegut, B. *J. Appl. Phys.* **1947**, *18*, 593.
(167) Langmuir, I. *Proc. Am. Philos. Soc.* **1948**, *92*, 167.
(168) Feibelman, P. J. *Science* **2002**, *295*, 99.
(169) Denzler, D. N.; Hess, C.; Dudek, R.; Wagner, S.; Frischkorn, C.; Wolf, M.; Ertl, G. *Chem. Phys. Lett.* **2003**, *376*, 618.
(170) Weissenrieder, J.; Mikkelsen, A.; Andersen, J. N.; Feibelman, P. J.; Held, G. *Phys. Rev. Lett.* **2004**, *93*, 196102.
(171) Andersson, K.; Nikitin, A.; Pettersson, L. G. M.; Nilsson, A.; Ogasawara, H. *Phys. Rev. Lett.* **2004**, *93*, 196101.
(172) Materzanini, G.; Tantardini, G. F.; Lindan, P. J. D.; Saalfrank, P. *Phys. Rev. B* **2005**, *71*, 155414.
(173) Haq, S.; Clay, C.; Darling, G. R.; Zimbitas, G.; Hodgson, A. *Phys. Rev. B* **2006**, *73*, 115414.
(174) Meng, S.; Wang, E. G.; Gao, S. *Phys. Rev. B* **2004**, *69*, 195404.
(175) Michaelides, A.; Alavi, A.; King, D. A. *J. Am. Chem. Soc.* **2003**, *125*, 2746.
(176) Faradzhev, N. S.; Kostov, K. L.; Feulner, P.; Madey, T. E.; Menzel, D. *Chem. Phys. Lett.* **2005**, *415*, 165.
(177) Morgenstern, M.; Müller, J.; Michely, T.; Comsa, G. *Z. Phys. Chem.* **1997**, *198*, 43.
(178) Meng, S.; Wang, E. G.; Frischkorn, C.; Wolf, M.; Gao, S. *Chem. Phys. Lett.* **2005**, *402*, 384.
(179) Clay, C.; Hodgson, A. *Curr. Opin. Solid State Mater. Sci.* **2005**, *9*, 11.
(180) Smith, R. S.; Kay, B. D. *Surf. Rev. Lett.* **1997**, *4*, 781.

(181) Stevenson, K. P.; Kimmel, G. A.; Dohnalek, Z.; Smith, R. S.; Kay, B. D. *Science* **1999**, *283*, 1505.
(182) Meyer, B.; Marx, D.; Dulub, O.; Diebold, U.; Kunat, M.; Langenberg, D.; Wöll, C. *Angew. Chem., Int. Ed.* **2004**, *43*, 6641.
(183) Brown, G. E., Jr.; Henrich, V. E.; Casey, W. H.; Clark, D. L.; Eggleston, C.; Felmy, A.; Goodman, D. W.; Grätzel, M.; Maciel, G.; McCarthy, M. I.; Nealson, K. H.; Sverjensky, D. A.; Toney, M. F.; Zachara, J. M. *Chem. Rev.* **1999**, *99*, 77.
(184) Wang, J.; Kalinichev, A. G.; Kirkpatrick, R. J. *Geochim. Cosmochim. Acta* **2006**, *70*, 562.
(185) Fahmi, A.; Minot, C. *Surf. Sci.* **1994**, *304*, 343.
(186) Zhao, J.; Li, B.; Jordan, K. D.; Yang, J.; Petek, H. *Phys. Rev. B* **2006**, *73*, 195309.
(187) Tilocca, A.; Selloni, A. *Langmuir* **2004**, *20*, 8379.
(188) Tilocca, A.; Selloni, A. *J. Phys. Chem. B* **2004**, *108*, 4743.
(189) Lindan, P. J. D.; Zhang, C. *Phys. Rev. B* **2005**, *72*, 075439.
(190) Diebold, U.; Ruzycki, N.; Herman, G. S.; Selloni, A. *Catal. Today* **2003**, *85*, 93.
(191) Henderson, M. A. *Surf. Sci.* **1996**, *355*, 151.
(192) Henderson, M. A. *Langmuir* **1996**, *12*, 5093.
(193) Herman, G. S.; Dohnalek, Z.; Ruzycki, N.; Diebold, U. *J. Phys. Chem. B* **2003**, *107*, 2788.
(194) Kunat, M.; Girol, S. G.; Burghaus, U.; Wöll, C. *J. Phys. Chem. B* **2003**, *107*, 14350.
(195) Diebold, U. *Surf. Sci. Rep.* **2003**, *48*, 53.
(196) Brookes, I. M.; Muryn, C. A.; Thornton, G. *Phys. Rev. Lett* **2001**, *87*, 266103.
(197) Bikondoa, O.; Pang, C. L.; Ithnin, R.; Muryn, C. A.; Onishi, H.; Thornton, G. *Nature Mater.* **2006**, *5*, 189.
(198) Wendt, S.; Matthiesen, J.; Schaub, R.; Vestergaard, E. K.; Laegsgaard, E.; Besenbacher, F.; Hammer, B. *Phys. Rev. Lett.* **2006**, *96*, 066107.
(199) Beck, T. J.; Klust, A.; Batzill, M.; Diebold, U.; Di Valentin, C.; Tilocca, A.; Selloni, A. *Surf. Sci.* **2005**, *591*, L267.
(200) Dulub, O.; Diebold, U.; Kresse, G. *Phys. Rev. Lett.* **2003**, *90*, 016102.
(201) Harris, L. A.; Quong, A. A. *Phys. Rev. Lett.* **2004**, *93*, 086105.
(202) Hugenschmidt, M. B.; Gamble, L.; Campbell, C. T. *Surf. Sci.* **1994**, *302*, 329.
(203) Brown, G. E., Jr. *Science* **2001**, *294*, 67.
(204) Wang, L.-Q.; Baer, D. R.; Engelhard, M. H.; Shultz, A. N. *Surf. Sci.* **1995**, *344*, 237.
(205) Himpsel, F. J. *Adv. Phys.* **1983**, *32*, 1.
(206) Plummer, E. W.; Eberhardt, W. *Adv. Chem. Phys.* **1982**, *49*, 533.
(207) Bisio, F.; Nyvlt, M.; Franta, J.; Petek, H.; Kirschner, J. *Phys. Rev. Lett.* **2006**, *96*, 087601.
(208) Wolf, M.; Hotzl, A.; Knoesel, E.; Velic, D. *Phys. Rev. B* **1999**, *59*, 5926.
(209) Petek, H.; Ogawa, S. *Annu. Rev. Phys. Chem.* **2002**, *53*, 507.
(210) Echenique, P. M.; Pendry, J. B. *J. Phys. C: Solid State Phys.* **1978**, *11*, 2065.
(211) Echenique, P. M.; Pendry, J. B. *Prog. Surf. Sci.* **1990**, *32*, 111.
(212) Zhu, X.-Y.; Vondrak, T.; Wang, H.; Gahl, C.; Ishioka, K.; Wolf, M. *Surf. Sci.* **2000**, *451*, 244.
(213) Ge, N. H.; Wong, C. M.; Harris, C. B. *Acc. Chem. Res.* **2000**, *33*, 111.
(214) Gahl, C. Ph.D. Thesis, Free University Berlin, Berlin, Germany, 2004.
(215) Dutton, G.; Pu, J.; Truhlar, D. G.; Zhu, X.-Y. *J. Chem. Phys.* **2003**, *118*, 4337.
(216) Andrianov, I.; Klamroth, T.; Saalfrank, P.; Bovensiepen, U.; Gahl, C.; Wolf, M. *J. Chem. Phys.* **2005**, *122*, 234710.
(217) Bezel, I.; Gaffney, K. J.; Garrett-Roe, S.; Liu, S. H.; Miller, A. D.; Szymanski, P.; Harris, C. B. *J. Chem. Phys.* **2004**, *120*, 845.
(218) Bovensiepen, U.; Li, B.; Sametoglu, V.; Kubo, A.; Petek, H. Unpublished results.
(219) Ryu, S.; Chang, J.; Kwon, H.; Kim, S. K. *J. Am. Chem. Soc.* **2006**, *128*, 3500.
(220) Hagfeldt, A.; Grätzel, M, *Acc. Chem. Res.* **2000**, *33*, 269
(221) Grätzel, M. *Nature* **2001**, *414*, 338.
(222) Maeda, K.; Teramura, K.; Lu, D.; Takata, T.; Saito, N.; Inoue, Y.; Domen, K. *Nature* **2006**, *440*, 295.
(223) Zou, Z.; Ye, J.; Sayama, K.; Arakawa, H. *Nature* **2001**, *414*, 625.
(224) Lewis, N. S. *Nature* **2001**, *414*, 589.
(225) Kurtz, R. L.; Stockbauer, R.; Madey, T. E.; Roman, E.; De Segovia, J. *Surf. Sci.* **1989**, *218*, 178.
(226) Heise, R.; Courths, R.; Witzel, S. *Solid State Commun.* **1992**, *84*, 599.
(227) See, A. K.; Thayer, M.; Bartynski, R. A. *Phys. Rev. B* **1993**, *47*, 13722.
(228) Onda, K.; Li, B.; Petek, H. *Phys. Rev. B* **2004**, *70*, 045415.
(229) Ino, D.; Watanabe, K.; Takagi, N.; Matsumoto, Y. *J. Phys. Chem. B* **2005**, *109*, 18018.
(230) Tang, H.; Levy, F.; Berger, H.; Schmid, P. E. *Phys. Rev. B* **1995**, *52*, 7771.
(231) Warren, D. S.; McQuillan, A. J. *J. Phys. Chem. B* **2004**, *108*, 19373.
(232) Minato, T.; Zhao, J.; Sainoo, Y.; Kim, Y.; Kato, H. S.; Kawai, M.; Aika, K.; Yang, J.; Petek, H. *Phys. Rev. Lett.* Manuscript submitted.
(233) Bredow, T.; Pacchioni, G. *Chem. Phys. Lett.* **2002**, *355*, 417.
(234) Bredow, T.; Aprà, E.; Catti, M.; Pacchioni, G. *Surf. Sci.* **1999**, *418*, 150.
(235) Ogawa, S.; Nagano, H.; Petek, H. *Phys. Rev. B* **1997**, *55*, 10869.
(236) Khomenko, V. M.; Langer, K.; Rager, H.; Fett, A. *Phys. Chem. Miner.* **1998**, *25*, 338.
(237) Henderson, M. A.; Epling, W. S.; Peden, C. H. F.; Perkins, C. L. *J. Phys. Chem. B* **2003**, *107*, 534.
(238) Winter, B.; Weber, R.; Widdra, W.; Dittmar, M.; Faubel, M.; Hertel, I. V. *J. Phys. Chem. A* **2004**, *108*, 2625.
(239) Li, B. Ph.D. Thesis, University of Pittsburgh, Pittsburgh, PA, 2006.
(240) Farfan-Arribas, E.; Madix, R. J. *Surf. Sci.* **2003**, *544*, 241.
(241) Henderson, M. A.; Otero-Tapia, S.; Castro, M. E. *Surf. Sci.* **1998**, *412−413*, 252.
(242) Zhang, Z.; Bondarchuk, O.; White, J. M.; Kay, B. D.; Dohnalek, Z. *J. Am. Chem. Soc.* **2006**, *128*, 4198.
(243) Henderson, M. A.; Otero-Tapia, S.; Castro, M. E. *Faraday Discuss. Chem. Soc.* **1999**, *114*, 313.
(244) Bisht, P. B.; Petek, H.; Yoshihara, K. *J. Chem. Phys.* **1995**, *103*, 5290.
(245) Hendry, E.; Wang, F.; Shan, J.; Heinz, T. F.; Bonn, M. *Phys. Rev. B* **2004**, *69*, 081101.
(246) Tributsch, H.; Pohlmann, L. *Science* **1998**, *279*, 1891.
(247) Cukier, R. I.; Nocera, D. G. *Annu. Rev. Phys. Chem.* **1998**, *49*, 337.
(248) Hammes-Schiffer, S. *Acc. Chem. Res.* **2001**, *34*, 273.
(249) Ferguson-Miller, S.; Babcock, G. T. *Chem. Rev.* **1996**, *96*, 2889.
(250) Madey, T. E. *Surf. Sci.* **1973**, *36*, 281.
(251) Decornez, H.; Hammes-Schiffer, S. *J. Phys. Chem. A* **2000**, *104*, 9370.
(252) Soudackov, A.; Hammes-Schiffer, S. *J. Chem. Phys.* **2000**, *113*, 2385.
(253) Echenique, P. M.; Pitarke, J. M.; Chulkov, E. V.; Rubio, A. *Chem. Phys.* **2000**, *251*, 1.
(254) Kavan, L.; Grätzel, M.; Gilbert, S. E.; Klemenz, C.; Scheel, H. J. *J. Am. Chem. Soc.* **1996**, *118*, 6716.
(255) Kawai, T.; Sakata, T. *J. Chem. Soc., Chem. Commun.* **1980**, 694.
(256) Dixon-Warren, S. J.; Jensen, E. T.; Polanyi, J. C. *Phys. Rev. Lett.* **1991**, *67*, 2395.
(257) Lu, Q. B.; Madey, T. E. *J. Chem. Phys.* **1999**, *111*, 2861.
(258) Lu, Q. B.; Sanche, L. *Phys. Rev. B* **2001**, *63*, 153403.
(259) Lu, Q. B.; Sanche, L. *Phys. Rev. Lett.* **2001**, *87*, 078501.
(260) Schnadt, J.; Bruehwiler, P. A.; Patthey, L.; O'Shea, J. N.; Soedergren, S.; Odelius, M.; Ahuja, R.; Karis, O.; Baessler, M.; Persson, P.; Siegbahn, H.; Lunell, S.; Martensson, N. *Nature* **2002**, *418*, 620.
(261) Huber, R.; Moser, J.-E.; Grätzel, M.; Wachtveitl, J. *J. Phys. Chem. B* **2002**, *106*, 6494.
(262) Stier, W.; Prezhdo, O. V. *J. Phys. Chem. B* **2002**, *106*, 8047.
(263) Rego, L. G. C.; Batista, V. S. *J. Am. Chem. Soc.* **2003**, *125*, 7989.
(264) Schwarzburg, K.; Ernstorfer, R.; Felber, S.; Willig, F. *Coord. Chem. Rev.* **2004**, *248*, 1259.

CR050173C